COSMOLOGICAL MODEL WITH A LOCAL VOID AND OBSERVATIONAL CONSTRAINTS

HO LE TUAN ANH

(B. Sc., College of Science, VNU, Vietnam, 2007)

A THESIS SUBMITTED

FOR THE DEGREE OF MASTER OF SCIENCE

DEPARTMENT OF PHYSICS

NATIONAL UNIVERSITY OF SINGAPORE

2009

Acknowledgements

I am deeply indebted to my supervisor Dr. Cindy Ng Shao Chin whose enthusiastic help, stimulating suggestions and kindness helped me in all the time of research and writing this thesis. I wish all the best coming to you and your family.

I would like to express my gratitude to my beloved family and friends for their constant supports, encouragement and care during the time I live in Singapore.

I also want to thank the National University of Singapore for the financial support to live and study in a wonderful country, Singapore.

Table of Contents

Summary

The ΛCDM model is widely accepted by most scientists and has achieved success in explaining observations and predicting cosmological properties, but there remain intrinsic and serious problems associated with the existence of the cosmological constant. Inspired by the revelation of a local void, many authors have proposed various inhomogeneous models as alternatives to the ΛCDM model. Among those inhomogeneous models, Tomita's model is a simple model, and in the late 1990s the model was shown to fit the Type Ia supernovae (Sne Ia) observations. In this work, Tomita's model is reanalyzed using the SCP Union compilation, which is the latest Sne Ia dataset. We find that for Tomita's model with an Einstein – de Sitter cosmology outside the local void and a zero cosmological constant density to provide a good fitting to the new data, the local void is on a scale of 1 Gpc, which is larger than the 200-Mpc scales from previous results. We then consider the Universe to be clumpy and find that the size of local void could be reduced if the clumpiness parameter α is less than 1, and for $\alpha = 0.5$ in particular, that the local void is about 700 Mpc ($z_{\text{boundary}} = 0.16$). In this work, we also find that the variations of the confidence contours and best-fit values with the model parameters are similar to those from Tomita's earlier analysis, but we further prove that the variations in the choice of the matter density profile and the clumpiness parameter of the local void are not significant.

List of Tables

List of Figures

CHAPTER 1
INTRODUCTION

Presently, with tremendous improvements of technology, astronomers can perform many observations with high accuracy. Type Ia supernovae (Sne Ia) observations, from which we can derive the magnitude – redshift relation, play important roles in constraining the cosmological parameters. In the late 1990s, the High-Redshift Supernova Search (HZS) [1, 2] and the Supernova Cosmology Project (SCP) [3] used Sne Ia observations to constrain the cosmological parameters. For a flat universe, the two teams found a model with 70% dark energy and 30% matter (the so-called Concordance Model). Similar results were found by further constraints from subsequent Sne Ia observations [4-8] and other independent observations, including the cosmic microwave background (CMB) anisotropy [9-11], the baryon acoustic oscillation (BAO) [12], the integrated Sachs – Wolfe (ISW) effect correlations [13]. In addition, the Concordance Model can explain accurately the relative abundance of light elements in later epochs, the age of the Universe, and the existence and thermal form of the CMB radiation.

However, the Concordance Model encounters several unresolved and critical issues. First, the Lambda-Cold Dark Matter (ΛCDM) model in which the dark energy is in the form of a cosmological constant is widely accepted by most scientists. In the Concordance Model, the cosmological constant is extremely small: about122 orders smaller than the expected value from quantum field theory. The

value of the cosmological constant is also fine-tuned. In the ΛCDM model, structure formation originated from the primordial fluctuations in a smooth background and grew into gravitationally bound systems such as galaxies and clusters. If the cosmological constant were slightly larger, the Universe would have expanded so fast that there would not have been t enough time for the formation of any gravitationally bound systems [14]. This is referred to as the cosmological constant problem.

The second issue is concerning the dark energy density. In an expanding Universe, the matter density decreases as the inverse third power of the cosmic scale factor $\left(\rho_{\mathrm{m}} \propto a^{-3}\right)$ and the cosmological constant energy density, remains constant in time. It is therefore an exceptional coincidence that the magnitudes of the two densities are of the same order at present. This issue is usually called the cosmic coincidence problem. The observed dimming in the Sne Ia apparent magnitudes has been explained by an acceleration in cosmic expansion, driven by the dark energy. The onset of the accelerating expansion is concomitant with the beginning of structure formation and it has been argued by some cosmologists that the latter could be the reason for the former [15-17].

The last problem is concerning the nature of the dark energy. At this point, we are still unsure as to what the dark energy is; we are unsure of its properties, how it has originated, and the method to detect it. There exist some models and theories of the dark energy but none of them is conclusive or proven by experiment (For a review, see [18]).

With the problems listed above, it is natural to question the correctness of the ΛCDM model, both observationally and theoretically. Theoretically, a value of

$\Lambda = 0$ may be more plausible than a minuscule one. In addition, based on the Cosmological Principle, the ΛCDM model assumes a spatially homogeneous and isotropic Friedmann-Lemaitre-Robertson-Walker (FLRW) metric for spacetime, which can be a good approximation in the early Universe when the density contrasts were very small. However, in later times when the Universe became more inhomogeneous with the presence of cosmic structures, ignoring the effect of inhomogeneity may lead to misinterpretation of the observational data and subsequently lead to the presence of a cosmological constant $\Lambda \neq 0$.

Recently, analyses of the number count of galaxies [19] and Sne Ia [20] have provided evidences that we may live in a local void. In addition, many voids with sizes of order Mpc and several huge nonlinear structures (notably, the Sloan Great Wall at $400/h$ Mpc) have been revealed through surveys like the Sloan Digital Sky Survey (SDSS) and the 2dF Galaxy Redshift Survey (2dFGRS) [21, 22]. Furthermore, voids can account for the cold spots [23-25] and some features of low multipole anomalies in the CMB data [26, 27]. With the development of high precision observations, we must account for all these inhomogeneous effects in our considerations.

In the realm of theoretical work, it was discovered that the metric averaging operation does not commute with the Einstein tensor calculating operation [28, 29]. In other words, we should use the exact metric to calculate the observable quantities and then take the average of the results, instead of the usual reversed procedure: take the average of the metric and then calculate the observable quantities from this averaged metric. In another work, Buchert found that in an inhomogeneous cosmology, the averaged quantities are subject to a set of modified Friedmann

equations – the Buchert equations – and the difference between the evolutions of homogeneous and inhomogenous models is characterized by a backreaction term due to the nonlinearity of the Einstein field equation [30-32]. Failure to account for the difference in overall dynamics between a perfect homogeneous Universe and an averaging one, or an underestimation of the selective light propagation effect in a clumpy Universe [33], could lead to incorrect conclusions of the nature of our Universe.

Besides the averaging approach, several cosmologists have introduced different cosmological models with a local void to interpret the observational data without invoking the dark energy or the cosmological constant component [33-40] (for a more complete review, see [41]). Due to the quasi-isotropy observed in the CMB radiation, these authors abandoned the Copernican Principle and assumed that we live near the centre of a spherical local void. For mathematical simplicity, they described the local void using the popular spherically symmetric LTB metric [42-44], which is an exact solution of the Einstein field equation. In these models, the inhomogeneity in energy density or structure distribution can affect light propagation, and the luminosity distance – redshift relation changes accordingly; by assuming an appropriate energy density profile, one can fit the Sne Ia data without dark energy. As of today, observational data is insufficient to distinguish different models, but can provide constraints on model parameters such as the size of the local void, matter density, and Hubble expansion rate. For example, Clifton *et al.* [45] found a local void of radius 1.3 Gpc, Garcia-Bellido and Haugboelle [38] found a local void of approximate size 2.5 Gpc, and Alexander *et al.* [34] found a minimal void of size about 350 Mpc, etc. Future observations may provide firmer constraints

on the size of the local void and rule out some of these models.

Grounded on the local void revelation, in the late 1990s, Tomita's [17, 36, 46] simple model proposes a spherical local void on scales of about 200 Mpc (The details of the model will be discussed in Chapter 2). In this framework, the author showed that the HZS [1, 2] and the SCP data [3] could be fit without a cosmological constant. Since then, many years have passed, and more Sne Ia data have now been obtained with higher accuracy. Also, in his original analysis [35], Tomita did not take into account the light propagation effect in a clumpy Universe. In this study, we will reinvestigate Tomita's model using the latest Sne Ia data, and we will also consider the general clumpy Universe in which the clumpiness (smoothness) parameter [47, 48] is different from unity.

This thesis is organized as followed: in Chapter 2, we introduce the model, the distance formula and the Sne Ia data fitting method. In Chapter 3, we perform the data fitting and show the results, including the confidence contours and the best-fit parameters, for both smooth and clumpy Universe. For comparison, we also consider a ΛCDM model with clumpiness effects in Chapter 3. In Chapter 4, we discuss the results and suggest possible future work. Chapter 5 is the thesis' conclusion. Finally, in the Appendix, we attach all the Matlab code used in this study. All programs are totally built by us from the very beginning.

CHAPTER 2
MODEL WITH A LOCAL VOID, THE LUMINOSITY DISTANCE-REDSHIFT RELATION, AND THE SNE IA DATA FITTING

2.1 Physical foundation of Tomita's model

In Chapter 1, it has been mentioned that we may live in a local void that is surrounded by huge nonlinear structures on scales of hundreds Mpc. Moreover, recent evidence shows that there exists anisotropy in the local Hubble flow [49], which would be a natural consequence if the local void is not completely spherical or we are not living right at the center. In addition, the value of local Hubble rate [50, 51] appears to be larger than the global value derived from the gravitational lensing and the Sunyaev – Zeldovich effect [52-55]. On this basis, Tomita [17, 36, 46] proposed a simple, spherically symmetric inhomogeneous cosmological model with a local void. This model consists of two homogeneous regions, inner and outer, separated by a singular spherical shell with zero thickness. The local void's matter density $\left(\Omega_{\mathrm{m\_in}}\right)$ is smaller than the outer region's matter density $\left(\Omega_{\mathrm{m\_out}}\right)$, and the mass of the shell is also assumed to compensate for the inner region's mass deficiency. The inner region can be easily corresponded to the local void and the shell corresponded to the filaments.

Before the epoch of structure formation, the Universe could be considered homogeneous, so the expansion rate (Hubble rate) was identical everywhere in the

Universe. Later, due to gravitational instability, under- and over-dense regions such as galaxy clusters, filaments, and voids gradually appear. The over-density region has stronger gravitational attraction and, accordingly, it causes a larger deceleration of the expansion rate than the under-density region does. Consequently, the expansion rate in the over-density region is smaller than that in the under-density region. In Tomita's model with a local void we have $\Omega_{\text{m\_in}} < \Omega_{\text{m\_out}}$, therefore, it is supposed that the inner Hubble rate (H_{in}) is always larger than the outer one (H_{out}). This assumption is in accord with the observations mentioned before.

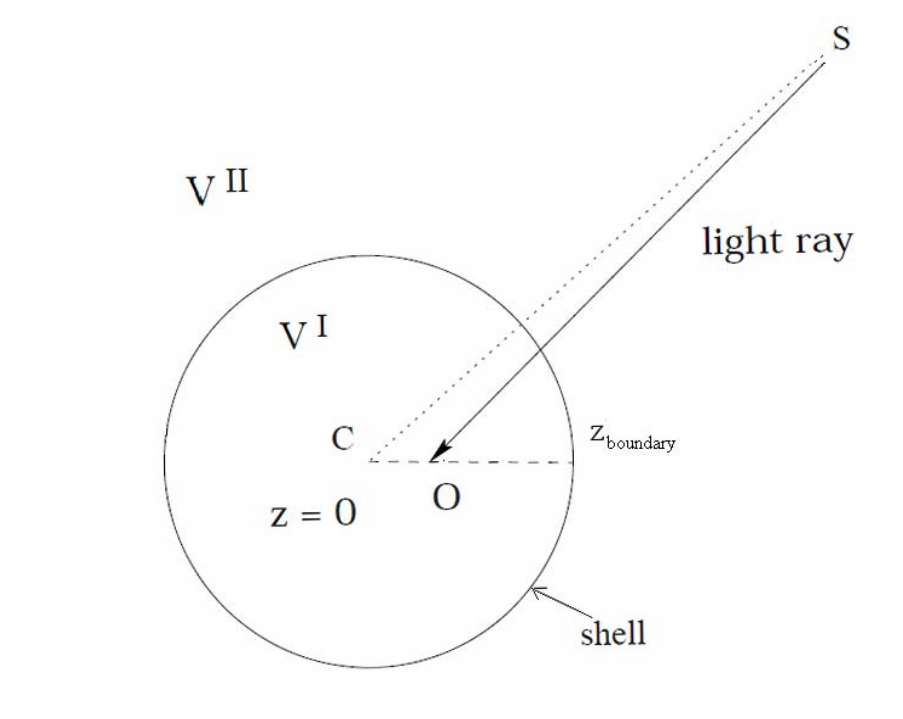

Figure 2.1 Tomita's model: V^{I} and V^{II} are the inner and outer region respectively, C is the centre of the void, O is the observer, S is the light source, and *z* is the redshift.

There seem to be some ambiguities in the assumptions made in Tomita's model. First, the shell is assumed to be thickness-free. In fact, the shell does have thickness, but its width is very small comparing to the radius of local void, hence we

can ignore the shell thickness. We can similarly ignore the distance CO between the observer and the void's centre (see Figure 2.1) because a large value of CO will cause a great CMB anisotropy which has not been observed. Therefore, for the rest of this thesis, the observer is assumed to be located at the centre. Beyond the local void, there exist many other under- and over-dense regions. Since most cosmological measurements are based on light propagation to us and are most strongly affected by the local void, for simplicity the outer region is assumed to be homogeneous to facilitate our computation.

During the late 90's of the last century, the accelerating expansion of the universe was discovered by two high redshift supernovae collaborations, the HZS [1, 2] and SCP [3]. The origin of this accelerating expansion has usually been ascribed to the influence of a nonzero cosmological constant in the ΛCDM framework. In this model, the accelerating expansion is a "real" phenomenon which is driven by the repulsive effect of the cosmological constant. Because the cosmological constant encounters aforementioned issues and its existence is, so far, not clearly evident, it may be necessary to search for different explanations in other ways, such as in the inhomogeneous framework.

To explain accelerating expansion in the inhomogeneous framework, the key concept is that when we observe distant objects, we not only look far in space but also look back in time. Mathematically, the variation of the Hubble rate with respect to redshift is the combination of a time-varying term and a space-varying term:

$$\left.\frac{dH}{dz}\right|_{t=t_0} = \left.\frac{\partial r}{\partial z}\frac{\partial H}{\partial r}\right|_{t=t_0} + \left.\frac{\partial t}{\partial z}\frac{\partial H}{\partial t}\right|_{t=t_0} \approx \frac{1}{H_0}\left.\left(\frac{\partial H}{\partial r} - \frac{\partial H}{\partial t}\right)\right|_{t=t_0} \tag{2.1}$$

In the last step, we have used the approximation for small distances: $\frac{\partial r}{\partial z} = \frac{1}{H_0}$, but

the conclusion below is valid even for larger value of r. In the homogeneous models, the Hubble rate depends only on the time variable t, so an increase in H at small z corresponds to a positive value of $\frac{\partial H}{\partial t}$ or an acceleration in the Universe's expansion. However, in the inhomogeneous framework the Hubble rate depends not only on the time t but also on the distance r, so a negative value of $\frac{dH}{dz}$ could be explained by a variation toward high expansion rate at the distance near the observer ($\frac{\partial H}{\partial r} < 0$) without imperative invocation of $\frac{\partial H}{\partial t} > 0$, or accelerating expansion, as one in the homogeneous framework. In particular, for Tomita's model, we can explain accelerating expansion as an apparent phenomenon: both regions in the model decelerate, but because the local void expands faster than the outer region, we perceive the Universe as if its expansion is accelerating.

In Tomita's model, to a good approximation, the metrics of spacetime in the two regions are presumed to be the homogeneous and isotropic FLRW metrics. The line-element is

$$\begin{aligned} ds^2 &= g^j_{\mu\nu}\left(dx^j\right)^\mu\left(dx^j\right)^\nu \\ &= -c^2\left(dt^j\right)^2 + \left[a^j\left(t^j\right)\right]^2\left\{\frac{\left(dr^j\right)^2}{1-k\left(r^j\right)^2} + r^2 d\Omega^2\right\} \end{aligned} \tag{2.2}$$

where

$j = I, II$ corresponds to the inner and outer region;

$g_{\mu\nu}$ is the metric of spacetime;

$c, a(t), r$ are the light velocity, scale factor and radial comoving

coordinate in FLRW cosmology, respectively;

$d\Omega^2 = d\theta^2 + \sin^2\theta\, d\varphi^2$ is the metric on a unit 2-sphere;

$k = (-1, 0, 1)$ is the curvature parameter corresponding to open, flat and close FLRW Universe.

2.2 Distances in Tomita's model

In Sne Ia observations, the quantities we measure from supernovae are distances and redshifts. In this study, our aim is to test the Tomita's model with the latest Sne Ia dataset and therefore, in this section, we will find the distance-redshift relation of this model. First we will derive the differential equation for the angular diameter distance, we then specify the initial conditions and solve the differential equation to find the angular diameter distance-redshift relation.

By definition, angular diameter distance d_a is proportional to the square root of the cross-sectional area A of a bundle of light geodesics, whose evolution is described by the Sachs optical scalar equations. The first of the Sachs optical scalar equations is [56]:

$$\frac{\partial\theta}{\partial\lambda} + \frac{1}{2}\theta^2 + \sigma^2 - \omega^2 + R_{\mu\nu}k^\mu k^\nu = 0 \tag{2.3}$$

In the equation above, θ, σ, ω are the expansion scalar, the shear, and the rotation of the bundle of light geodesics, respectively. λ is the affine parameter along the light geodesics. $R_{\mu\nu}$ is the Ricci tensor and $k^\mu = \frac{\partial x^\mu}{\partial\lambda}$ is the wave-vector of the light ray (the tangent vector of the light geodesics). In this work, unless noted explicitly, the Latin-based indexes $i, j, k...$ are of the range $(1, 2, 3)$ and Greek-based indexes

$\alpha, \beta, \mu, \nu ...$ are of the range $(0,1,2,3)$. The expansion scalar θ is a measure of the fractional rate of change of A (see Chapter 2 of [57]), and it follows that

$$\theta = \frac{1}{A}\frac{\partial A}{\partial \lambda} = \frac{2}{\sqrt{A}}\frac{\partial\left(\sqrt{A}\right)}{\partial \lambda} = \frac{2}{d_a}\frac{\partial d_a}{\partial \lambda} \tag{2.4}$$

For a bundle of light geodesics, the shear term represents the tendency of an initial circular cross section to be distorted into ellipse shape, and the rotation term represents its tendency to rotate. In Tomita's model, due to the spherically symmetric metric and center located observer, the light ray travels along the path of constant inclination and azimuth angle in spherical coordinate system. Therefore, the shear and rotation term: $\sigma = \omega = 0$. Eq. (2.3) then becomes:

$$\frac{\partial \theta}{\partial \lambda} + \frac{1}{2}\theta^2 + R_{\mu\nu}k^\mu k^\nu = 0 \tag{2.5}$$

Substituting Eq. (2.4) into Eq. (2.5) and simplifying the equation, we get:

$$\frac{\partial^2 d_a}{\partial \lambda^2} = -\frac{1}{2}R_{\mu\nu}k^\mu k^\nu d_a \tag{2.6}$$

Notice that the light path is null geodesic. We now have:

$$g_{\mu\nu}k^\mu k^\nu = 0 \tag{2.7}$$

Substituting the Einstein field equation $R_{\mu\nu} = \frac{8\pi G}{c^4}\left(T_{\mu\nu} - \frac{1}{2}Tg_{\mu\nu}\right) + \Lambda g_{\mu\nu}$ into the right hand side of Eq. (2.6) and using the null condition in Eq. (2.7), we obtain:

$$\begin{aligned} R_{\mu\nu}k^\mu k^\nu &= \left[\frac{8\pi G}{c^4}\left(T_{\mu\nu} - \frac{1}{2}Tg_{\mu\nu}\right) + \Lambda g_{\mu\nu}\right]k^\mu k^\nu \\ &= \frac{8\pi G}{c^4}\left(T_{\mu\nu}k^\mu k^\nu - \frac{1}{2}Tg_{\mu\nu}k^\mu k^\nu\right) + \Lambda g_{\mu\nu}k^\mu k^\nu = \frac{8\pi G}{c^4}T_{\mu\nu}k^\mu k^\nu \end{aligned} \tag{2.8}$$

For late time Universe, the radiation energy is very small comparing to other energy components. Therefore, we assume that the Universe only contains dark

energy in the form of a cosmological constant and irrotational dust behaving like an ideal fluid. The stress-energy tensor is

$$T_{\mu\nu} = \left(\rho + \frac{p}{c^2}\right) u_\mu u_\nu + p g_{\mu\nu} \tag{2.9}$$

where u, p, ρ are respectively the four-velocity, pressure and density of the fluid.

In comoving coordinates we have

$$\begin{aligned} &\rho = \rho_m + \rho_\Lambda ; \\ &p = p_m + p_\Lambda ; p_m = 0; p_\Lambda = -\rho_\Lambda c^2; \\ &u_0 = g_{0\alpha} u^\alpha = -c; \\ &u_i = 0; \end{aligned} \tag{2.10}$$

Also for late time, the Universe has evolved under gravitational instability from a homogeneous state into a clumpy state where matter accreted into different structures (such as galaxies, clusters, etc.) and the space between these matter clumps becomes a void of with low matter density. Light traveling through emptier space is more likely to be detect by observations; physically, the emptier a region, the more easily the photons travel through and arrive at the observer without being absorbed or scattered. Moreover, light from objects which lie behind galaxies is often contaminated, and thus data analyses usually remove these objects because of the large resulting uncertainty. This creates a bias in Sne Ia observations in favor of light which has travelled through emptier regions. Due to these reasons, we suppose that light reaching us mostly propagates through intergalactic medium. Therefore, all terms in Eq. (2.3) and Eq. (2.10) must be determined on light geodesics in the intergalactic medium. Assuming that the intergalactic medium has a mean matter density a fraction α $\left(0 \le \alpha \le 1\right)$ of the Universe's mean matter density

$$\rho_m = \alpha \rho_{mean\_Universe} = \alpha \rho_{0m} / a^3 \tag{2.11}$$

where ρ_{0m} is the mean matter density of the whole Universe at present, $a \equiv a(t)$ is the scale factor, α is the clumpiness parameter, Eq. (2.8) becomes

$$\begin{aligned} R_{\mu\nu} k^\mu k^\nu &= \frac{8\pi G}{c^4} T_{\mu\nu} k^\mu k^\nu = \frac{8\pi G}{c^4} \left[\left(\rho + \frac{p}{c^2} \right) u_\mu u_\nu + p g_{\mu\nu} \right] k^\mu k^\nu \\ &= \frac{8\pi G}{c^4} \left(\rho_m + \rho_\Lambda - \frac{\rho_\Lambda c^2}{c^2} \right) u_\mu u_\nu k^\mu k^\nu \\ &= \frac{8\pi G}{c^4} \rho_m u_\mu u_\nu k^\mu k^\nu = \frac{8\pi G \alpha \rho_{0m}}{c^2 a^3} k^0 k^0 \end{aligned} \tag{2.12}$$

Now, to find the time-component of the light wave-vector k^0, we use the geodesic equation (Eq. (9.47) in [58])

$$\frac{d}{d\lambda} \left(g_{\alpha\beta} \frac{dx^\beta}{d\lambda} \right) = \frac{1}{2} \frac{\partial g_{\beta\gamma}}{\partial x^\alpha} \frac{dx^\beta}{d\lambda} \frac{dx^\gamma}{d\lambda} \tag{2.13}$$

Where $g_{\alpha\beta} = diag\left(-1, \frac{a(t)^2}{1-kr^2}, a(t)^2 r^2, a(t)^2 r^2 \sin^2(\theta) \right)$ as in the line element (2.2).

We only want to find k^0 so we substitute the index $\alpha = 0$ into Eq. (2.13):

$$\begin{aligned} & \frac{d}{d\lambda} \left(g_{0\beta} \frac{dx^\beta}{d\lambda} \right) = \frac{1}{2} \frac{\partial g_{\beta\gamma}}{\partial x^0} \frac{dx^\beta}{d\lambda} \frac{dx^\gamma}{d\lambda} \\ \Leftrightarrow \quad & \frac{d}{d\lambda} \left(g_{00} \frac{dx^0}{d\lambda} \right) = \frac{1}{2} \dot{g}_{\alpha\alpha} k^\alpha k^\alpha \\ \Leftrightarrow \quad & -\frac{dk^0}{c\,dt} \frac{d(ct)}{d\lambda} = \frac{1}{2} \dot{g}_{\alpha\alpha} k^\alpha k^\alpha \\ \Leftrightarrow \quad & -\frac{dk^0}{dt} = \frac{1}{2} \frac{c\,\dot{g}_{\alpha\alpha} k^\alpha k^\alpha}{k^0} \end{aligned} \tag{2.14}$$

From the form of $g_{\alpha\beta}$ above, it follows that $\dot{g}_{\alpha\beta} = diag\left(0, 2\frac{\dot{a}}{a} g_{ii} \right)$, substituting this

expression into the right hand side of Eq. (2.14), the equation becomes:

$$\frac{dk^0}{dt} = -cg_{ii}\frac{k^i k^i}{k^0}\frac{\dot{a}}{a} \tag{2.15}$$

From Eq. (2.7) we derive the relation:

$$g_{ii}k^i k^i = -g_{00}k^0 k^0 \tag{2.16}$$

Therefore, Eq. (2.15) becomes

$$\frac{dk^0}{dt} = -ck^0\frac{\dot{a}}{a} \tag{2.17}$$

Separate the variables and integrate both sides of Eq. (2.17), we find

$$\begin{aligned} k^0 &\equiv \frac{dx^0}{d\lambda} = \frac{C}{a} \\ x^0 &\equiv ct, \quad C \equiv const. \end{aligned} \tag{2.18}$$

Since λ is an affine parameter, we could multiply λ by a constant factor without affecting the physical results, hence the constant C could be chosen arbitrarily. If we choose $C = \frac{c}{H_0}$ (Hubble radius), Eq. (2.18) then becomes:

$$k^0 = \frac{c}{H_0 a} \tag{2.19}$$

Substitute Eq. (2.19) into Eq. (2.12), we have:

$$\begin{aligned} R_{\mu\nu}k^\mu k^\nu &= \frac{8\pi G\alpha\rho_{0m}}{c^2 a^3}\left(\frac{c}{H_0 a}\right)^2 \\ &= \frac{\rho_{0m}}{\left(3H_0^2/8\pi G\right)}\frac{3\alpha}{a^5} \\ &= 3\alpha\Omega_{0m}\left(1+z\right)^5 \end{aligned} \tag{2.20}$$

Where Ω_{0m} is the present matter density in the unit of the critical density, in the last

step, we have also used the relation $1+z=\frac{1}{a}$. Substituting Eq. (2.20) into Eq. (2.6), we now have

$$\frac{\partial^2 d_a}{\partial \lambda^2} = -\frac{3}{2}\alpha\Omega_{0m}(1+z)^5 d_a \tag{2.21}$$

To obtain the differential equation of the angular distance d_a with respect to the redshift z, we must find the relation between the affine parameter λ and the redshift z. From (2.19), we have:

$$\frac{dt}{d\lambda} = \frac{1}{H_0 a(t)} \tag{2.22}$$

Differentiating both sides of the equation $1+z=\frac{1}{a(t)}$, we have

$$dz = -\frac{\dot{a}(t)}{a^2(t)}dt \tag{2.23}$$

Combining (2.22) and (2.23), we have

$$\begin{aligned} dz &= -\frac{\dot{a}(t)}{a(t)}\frac{1}{H_0 a^2(t)}d\lambda \\ &= -\frac{H}{H_0 a^2(t)}d\lambda \end{aligned} \tag{2.24}$$

In FLRW cosmology,

$$H = H_0\sqrt{\frac{\Omega_{0m}}{a^3}+\Omega_{0\Lambda}+\frac{1-\Omega_{0m}-\Omega_{0\Lambda}}{a^2}} \tag{2.25}$$

Hence, Eq. (2.24) becomes

$$\begin{aligned} \frac{dz}{d\lambda} &= -\frac{\sqrt{\Omega_{0m}/a^3+\Omega_{0\Lambda}+(1-\Omega_{0m}-\Omega_{0\Lambda})/a^2}}{a^2(t)} \\ &= -(1+z)^2\sqrt{\Omega_{0m}(1+z)^3+\Omega_{0\Lambda}+(1-\Omega_{0m}-\Omega_{0\Lambda})(1+z)^2} \end{aligned} \tag{2.26}$$

Therefore

$$\frac{\partial d_a}{\partial \lambda} = \frac{dd_a(\lambda)}{d\lambda} = \frac{dd_a(z)}{dz}\frac{dz}{d\lambda}$$
$$= -(1+z)^2 \sqrt{\Omega_{0m}(1+z)^3 + \Omega_{0\Lambda} + (1-\Omega_{0m}-\Omega_{0\Lambda})(1+z)^2}\,\frac{dd_a(z)}{dz}$$

Differentiate equation above with respect to λ, we have

$$\frac{\partial^2 d_a}{\partial \lambda^2} = \frac{d^2 d_a(\lambda)}{d\lambda^2} = \frac{d}{dz}\left(\frac{dd_a}{dz}\right)\frac{dz}{d\lambda}$$
$$= (1+z)^4 F \frac{d^2 d_a}{dz^2} \tag{2.27}$$
$$+ (1+z)^3 \left\{2F + \frac{1}{2}(1+z)^2\left[\Omega_{0m}(1+3z) + 2 - 2\Omega_{0\Lambda}\right]\right\}\frac{dd_a}{dz}$$

where

$$F \equiv (1+\Omega_{0m}z)(1+z)^2 - \Omega_{0\Lambda}z(2+z) \tag{2.28}$$

Substituting Eq. (2.27) into Eq. (2.21), simplifying the resulting equation, and adding the index $j = I, II$ to specify the inner and outer region, we obtain the differential equation for angular diameter distance in Tomita's cosmology, which also take into account the clumpiness along path:

$$\frac{d^2\left(d_a^j\right)}{d\left(z^j\right)^2} + \left\{\frac{2}{1+z^j} + \frac{1}{2}\left(1+z^j\right)\left[\Omega_{0m}^j\left(1+3z^j\right) + 2 - 2\Omega_{0\Lambda}^j\right]F^{-1}\right\}\frac{d\left(d_a^j\right)}{dz^j}$$
$$+ \frac{3}{2}\Omega_{0m}^j \alpha\left(1+z^j\right)F^{-1}d_a^j = 0 \tag{2.29}$$

Eq. (2.29) is a second order differential equation and solving this equation analytically is quite difficult, so we will solve it numerically. In the following, we determine the necessary initial conditions for solving this differential equation.

First, we have the junction conditions at the shell:

$$z_1^I = z_1^{II} \equiv z_1 \tag{2.30}$$

$$d_a^I\Big|_{z^I=z_1} = d_a^{II}\Big|_{z^{II}=z_1} \tag{2.31}$$

To find the angular diameter distance in the inner region *I*, we solve Eq. (2.28) using the initial conditions:

$$\begin{cases} d_a^I\Big|_{z^I=0} = 0 \\ \dfrac{dd_a^I}{dz^I}\Big|_{z^I=0} = \dfrac{c}{H_0^I} \end{cases} \tag{2.32}$$

Finding the angular diameter distance in the outer region *II* is slightly more complicated. First, we solve Eq. (2.29) using the conditions:

$$\begin{cases} d_a^{II}\Big|_{z^{II}=z_1} = d_a^I\Big|_{z^I=z_1} \\ \dfrac{dd_a^{II}}{dz^{II}}\Big|_{z^{II}=0} = \dfrac{c}{H_0^{II}} \end{cases} \tag{2.33}$$

and find the value $\left.\dfrac{dd_a^{II}}{dz^{II}}\right|_{z^{II}=z_1}$ (2.34). Then by using (2.34) and (2.31) as initial conditions, we solve Eq. (2.28) for $d_a^{II}\left(z^{II}\right)$ in the range $\left(z_1,+\infty\right)$. The final angular diameter distance is defined as:

$$d_a(z) = \begin{cases} d_a^I(z) & \text{for } z \le z_1 \\ d_a^{II}(z) & \text{for } z > z_1 \end{cases} \tag{2.35}$$

The luminosity distance is readily calculated by the relation:

$$d_L(z) = (1+z)^2\, d_a(z) \tag{2.36}$$

2.3 Cosmological constraints using Sne Ia samples

In observations, astronomers prefer using distance modulus μ to express the distance. This quantity is related to the luminosity distance by the formula

$$\mu = 5\log\left(\frac{d_L}{\text{Mpc}}\right) + 25 \tag{2.37}$$

Alternatively, the distance modulus μ is determined from two empirically defined quantities, absolute magnitude M and apparent magnitude m of a luminous object:

$$\mu = m - M \tag{2.38}$$

The apparent magnitude m is commonly measured in the B-band spectrum.

From Eq. (2.37) we could theoretically derive values of distance modulus from luminosity distance calculated in Eq. (2.36). Besides, from Eq. (2.38) we also have observationally determined values. Therefore, we can fit the distance modulus to the Sne Ia sample, find the goodness-of-fit and constrain the model parameters using Bayesian analysis:

$$\chi^2 = \sum_{i=1}^{N} \frac{\left(\mu_{\text{obs},i} - \mu_{\text{the}}\left(z_i\right)\right)^2}{\sigma_i^2} \tag{2.39}$$

where

$\mu_{\text{obs},i}, \mu_{\text{the}}\left(z_i\right)$ are the observed and theoretically derived distance modulus,

N is the number of Sne Ia in the sample,

σ_i is the measurement error of the distance modulus at redshift z_i

The corresponding probability distribution function (PDF) is proportional to the exponent of $-\chi^2/2$:

$$p(\text{pars}) \propto \exp\left(-\frac{1}{2}\chi^2\right) \tag{2.40}$$

where pars are cosmological parameters of the model.

In Tomita's model there are 7 parameters: Hubble constant and matter density in the inner and outer region, $H_{\text{in}} \equiv H_0^I, H_{\text{out}} \equiv H_0^{II}, \Omega_{\text{in}} \equiv \Omega_{0m}^I, \Omega_{\text{out}} \equiv \Omega_{0m}^{II}$, outer dark energy density in the form of cosmological constant, $\Omega_\lambda \equiv \Omega_{0\Lambda}^{II}$ (Because $\Lambda = 3\left(H_0^I\right)^2 \Omega_{0\Lambda}^I = 3\left(H_0^{II}\right)^2 \Omega_{0\Lambda}^{II}$, the inner dark energy density could be directly calculated from the outer one by the formula: $\Omega_{0\Lambda}^I = \left(\frac{H_0^{II}}{H_0^I}\right)^2 \Omega_{0\Lambda}^{II} \equiv \left(\frac{H_{\text{out}}}{H_{\text{in}}}\right)^2 \Omega_\lambda$), the redshift of the local void boundary, z_1, and the clumpiness parameter, α. In order to compare Tomita's model with the observational data from supernovae samples, we must find the magnitude – redshift relation of the Tomita's model. This requires us to numerically solve the second order differential equation (2.29) repeatedly, for different values of the parameter set $\left(H_{\text{in}}, H_{\text{out}}, \Omega_{\text{in}}, \Omega_{\text{out}}, \Omega_\lambda, z1, \alpha\right)$ over the physical range of the parameter space. It is indeed too complicated, if not to say impossible, for contemporary computational power to solve the differential equation numerous times if we keep fitting 7 parameters simultaneously. Therefore, we will follow [35, 36] and consider some specific values of $R \equiv H_{\text{out}}/H_{\text{in}}$, z_1, Ω_{in}, and α, hence reduce the number of free parameters to three. We then compute the probability $p\left(\Omega_{\text{out}}, \Omega_\lambda\right)$ by marginalizing the likelihood $p\left(\Omega_{\text{out}}, \Omega_\lambda, H_{\text{in}}\right)$ over the inner Hubble constant H_{in} (the "nuisance" parameter),

$$p\left(\Omega_{\text{out}}, \Omega_\lambda\right) = \int p\left(\Omega_{\text{out}}, \Omega_\lambda, H_{\text{in}}\right) dH_{\text{in}} \tag{2.41}$$

where

$$p\left(\Omega_{\text{out}},\Omega_{\lambda},H_{\text{in}}\right)=\frac{\exp\left(-\frac{1}{2}\chi^{2}\left(\Omega_{\text{out}},\Omega_{\lambda},H_{\text{in}}\right)\right)}{\int\exp\left(-\frac{1}{2}\chi^{2}\left(\Omega_{\text{out}},\Omega_{\lambda},H_{\text{in}}\right)\right)d\Omega_{\text{out}}d\Omega_{\lambda}dH_{\text{in}}} \tag{2.42}$$

or equivalently,

$$\chi^{2}\left(\Omega_{\text{out}},\Omega_{\lambda}\right)=-2\ln\left(\int\exp\left(-\frac{1}{2}\chi^{2}\left(\Omega_{\text{out}},\Omega_{\lambda},H_{\text{in}}\right)\right)dH_{\text{in}}\right) \tag{2.43}$$

We use $\chi^{2}\left(\Omega_{\text{out}},\Omega_{\lambda}\right)$ to plot the confidence contours. The pair $\left(\Omega_{\text{out}},\Omega_{\lambda}\right)$ corresponding to χ^{2}_{min} is the best-fit value of the model.

There have been many Sne Ia compilations, with the SCP Union compilation (Table 11 in [8]) being the most updated by far. Contrasting many previous compilations which combined various datasets of different lightcurve fitting functions and analysis procedures, SCP Union compilation uses only one method for all the Sne Ia samples it includes. Therefore, it is also the most self-consistent dataset up to now. In this work, our data fitting mainly uses the SCP Union compilation. Following Kowalski *et al.* [8], throughout this work we employ only 307 Sne Ia which pass the 3σ outlier cut. The reason of this outlier cut selection is explained in section 4.3 of Kowalski *et al.* [8].

CHAPTER 3
DATA FITTING AND THE RESULTS

In this chapter, we will show that the Tomita's model can fit the SCP Union compilation even without the cosmological constant component. Besides, it is found that standard parameters used in Tomita's paper [35] are inconsistent with the new dataset, and new standard parameters are found accordingly. We will also investigate the variation of the best-fit values and confidence contours with the model parameters, in both smooth and clumpy Universe.

3.1 Standard parameters

As mentioned in previous section, we will use some specific values of $R \equiv H_{\text{out}}/H_{\text{in}}$, z_1, Ω_{in}, and α. In Table 1, we list some matter density profiles which will be used in this thesis. For profiles A, it satisfies the condition that the outer matter density is always greater than the inner matter density. In addition, it is also consistent with the local matter density obtained from other measurements: $\Omega_{\text{m\_local}} \approx 0.3$ (in critical density unit). Tomita, in his paper [35], has used profile A as standard for data fitting. Apart from profile A, profile B has the same matter density $\rho = \Omega_0^j \frac{3\left(H_0^j\right)^2}{8\pi G}$ for both inner and outer region and Profile C, D have different constant values of inner matter density.

Profile	Ω_{in}
A	$\Omega_{in} = \Omega_{out}/2$ if $\Omega_{out} < 0.6$; $\Omega_{in} = 0.3$ if $\Omega_{out} \geq 0.6$
B	$\Omega_{in} = \Omega_{out} R^2$
C	$\Omega_{in} = 0.3 \ \forall \ \Omega_{out}$
D	$\Omega_{in} = 0.2 \ \forall \ \Omega_{out}$

Table 1. Four matter density profiles

First, we consider matter density profile A and a smooth Universe ($\alpha = 1$). Applying the data-fitting method described in Section 2.3 and using Matlab (the code is shown in the Appendix I), we vary parameter R and z_1 and find the values $R = 0.69$ and $z_1 = 0.23$ give a good fit to the new SCP Union dataset, with zero cosmological constant density and flat Einstein – de Sitter cosmology outside the local void. This result resolves the puzzle of cosmological constant and it accords closely with the flat Universe from CMB observations. In the rest of this chapter, we will use these parameter values as our standard parameters.

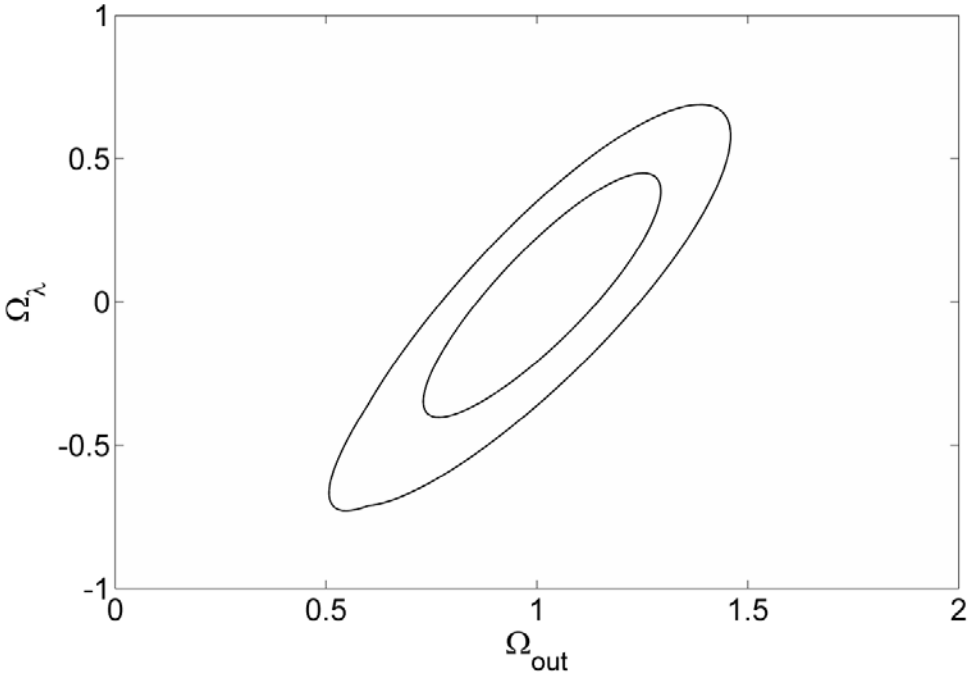

Figure 3.1 68.3% and 95.4% confidence contours in $\Omega_{out} - \Omega_\lambda$ plane, for $R = 0.69$, $z_1 = 0.23$, matter density profile A and $\alpha = 1$

In Figure 3.1, the contours of 68.3% and 95.4% confidence levels (CLs) are plotted. As expected, the contours centre at $(\Omega_{\text{out}},\Omega_{\lambda})=(1,0)$. The minimum χ^2 is 316.04 with 305 degrees of freedom. Accordingly, the goodness-of-fit is about 32%, which is quite a good fit. The best-fit values corresponding to the minimum $\chi^2(\Omega_{\text{out}},\Omega_{\lambda},H_{\text{in}})$ are $(\Omega_{\text{out}},\Omega_{\lambda},H_{\text{in}})=(1.02^{+0.18}_{-0.19},0.04^{+0.28}_{-0.29},68.7^{+0.7}_{-0.7})$ where the errors include only the statistical uncertainties. As can be seen, our derived best-fit local Hubble parameter is in good agreement with the observational measurement from the Hubble Space Telescope Project [51]: $H=72^{+8}_{-8}$ km/s.Mpc.

To visualize the fitting, in Figure 3.2 we plot the residual Hubble diagram for our best-fit model and the binned observational data (SCP Union compilation), assuming H_0 = 68.5 km/s/Mpc. Here we use uniform and unbiased binning with a fixed value of $n\Delta z=10$, where n is the number of Sne Ia in a redshift bin and Δz is the bin width. For the Sne Ia in each bin, we calculate the weighted mean of their redshifts $\langle z\rangle_i$, residual distance modulus $\langle\Delta\mu\rangle_i$ and standard deviation $\langle\sigma\rangle_i$ as follows:

$$\langle z\rangle_i=\frac{\sum_{j=1}^{N_i}z_j}{N_i},\quad \langle\Delta\mu\rangle_i=\frac{\sum_{j=1}^{N_i}\left(\mu_j-\mu_{\text{Milne},j}\right)/\sigma_j^2}{\sum_{j=1}^{N_i}\left(1/\sigma_j^2\right)},\quad \langle\sigma\rangle_i=\frac{1}{\sqrt{\sum_{j=1}^{N_i}\left(1/\sigma_j^2\right)}} \tag{2.44}$$

Where N_i is the number of Sne Ia in i$^{\text{th}}$ bin; $\mu_j,\sigma_j,\mu_{\text{Milne},j}$ are respectively the observational distance modulus, standard deviation and theoretical distance modulus in empty Milne Universe at redshift z_j.

After binning, we have seven bins for the SCP Union compilation with the means in each bin listed in Table 2. We also plot the ΛCDM model in the same

figure for comparison. Matlab programs for this process is provided in the Appendix.

Bin	$z_{initial} - z_{final}$	$\langle z \rangle$	$\langle \Delta\mu \rangle$	$\langle \sigma \rangle$
1	0 – 0.174	0.044	– 0.0188	0.0175
2	0.174 – 0.388	0.317	0.0672	0.0267
3	0.388 – 0.531	0.463	0.1182	0.0269
4	0.531 – 0.702	0.610	0.0868	0.0282
5	0.702 – 0.927	0.809	0.0712	0.0382
6	0.927 – 1.300	1.035	– 0.0374	0.0579
7	1.300 – 1.551	1.391	– 0.1911	0.1472

Table 2. Redshift range, weighted mean of redshift, distance modulus and standard deviation of each bin of SCP Union compilation.

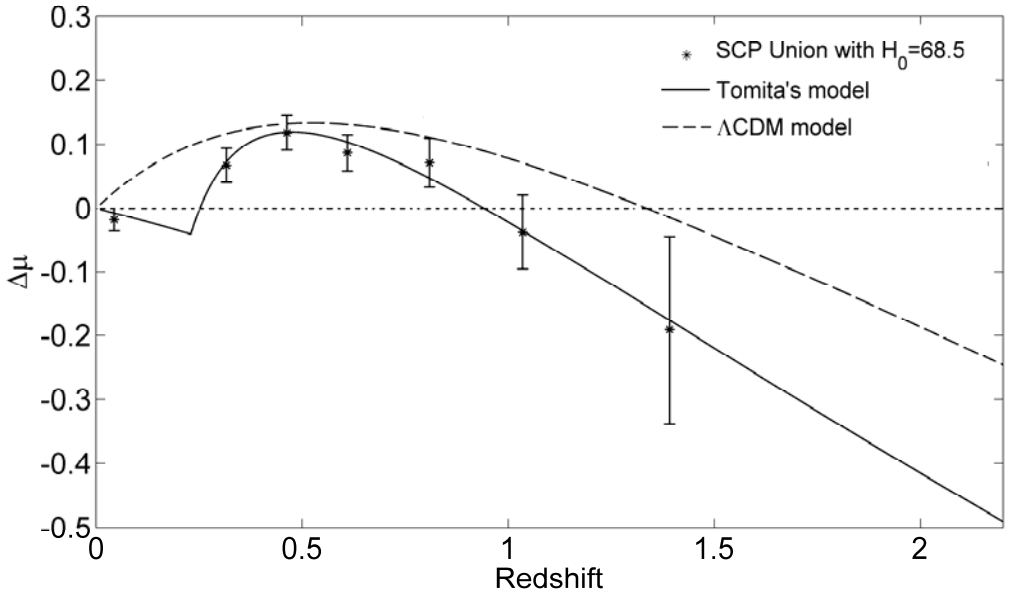

Figure 3.2 The $\Delta\mu - z$ diagram for Tomita's model with the standard parameters and the ΛCDM model, compared to the binned observational data. The dotted horizontal line corresponds to the empty Milne Universe.

In Tomita's earlier analyses [35], the older datasets were used and the standard parameters were $(R, z_1) = (0.80, 0.08)$ for matter density profile A. For comparison, in Figure 3.3 we plot the new confidence contours for these former

standard parameters. From the figure we see that the point $(\Omega_{\text{out}}, \Omega_{\lambda}) = (1, 0)$ lies far beyond the 2σ confidence region. Thus, with the former standard parameters, a model with zero cosmological constant and flat cosmology in the outer region is ruled out at 2-sigma level. The local void size and Hubble rate's disparity associated with the former standard parameters are simply too small.

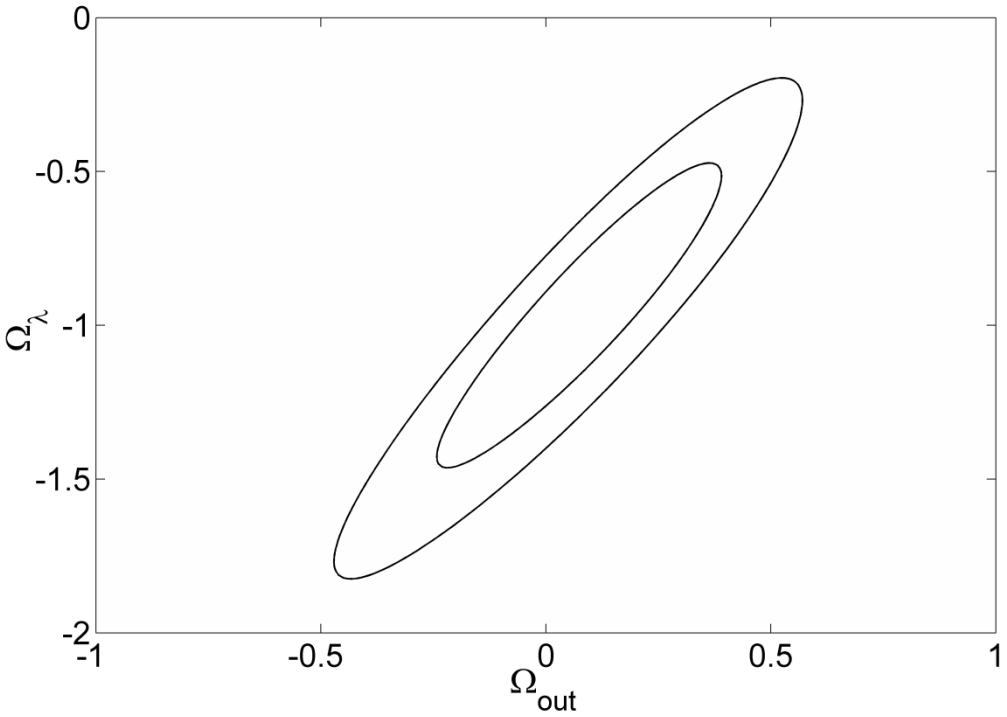

Figure 3.3 68.3% and 95.4% confidence contours in $\Omega_{\text{out}} - \Omega_{\lambda}$ plane, for $R = 0.80$, $z_1 = 0.08$, matter density profile A and $\alpha = 1$.

To see how tight the parameters constraint has changed since the first analyses by Tomita up to present by ours, in Figure 3.4, we plot the 95.4% confidence level contours for three different datasets: the Riess 98 sample [1, 2] which is used by Tomita in his earlier analyses [35] with 50 Sne Ia, the Gold sample [6] with 182 Sne Ia, and the SCP Union compilation [8] with 307 Sne Ia. The standard parameters in Figure 3.1 are used. Our calculations show that 95.4% CL confidence contour's area of the SCP Union compilation is about 60% that of the

Gold sample, which is about 11.5 times less than that of the Riess 98 sample. As expected, when the number of Sne Ia increases from one dataset to another, the constraint tightens progressively.

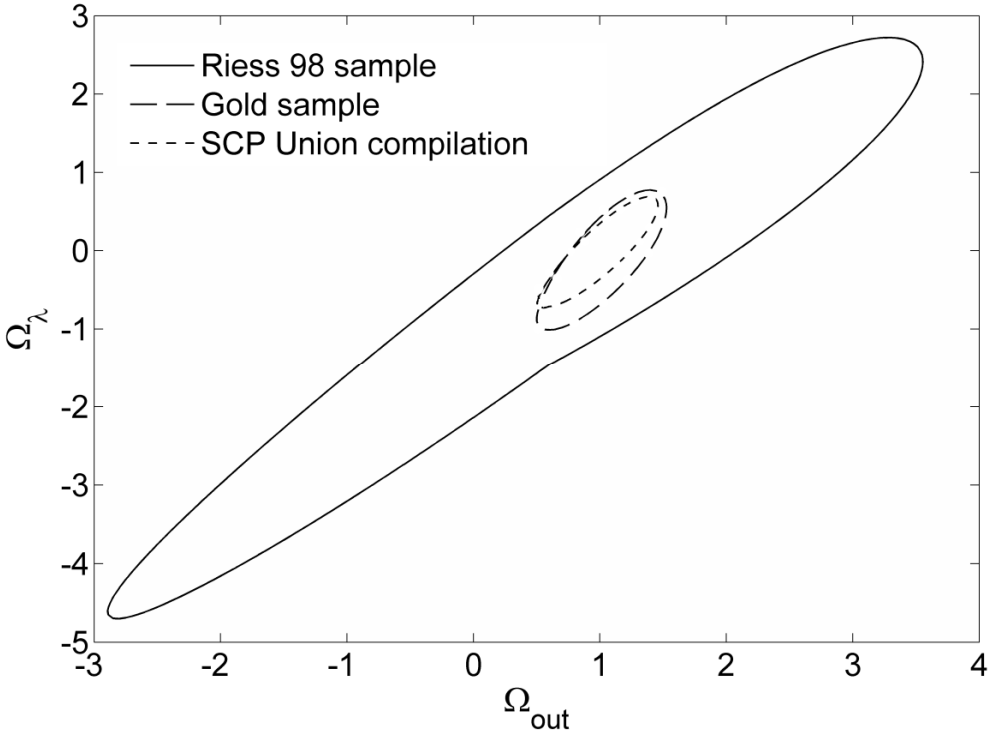

Figure 3.4 95.4% confidence level contours for Riess 98 sample, Gold sample (2007), and SCP Union compilation (2008), for $R = 0.69$, $z_1 = 0.23$, matter density profile A, and $\alpha = 1$

3.2 Variation of confidence contours with model parameters

In this section, we follow Tomita's earlier analyses [35] and examine the variation of the confidence contours as the model parameters vary from their standard values. We vary the parameters as follows: Hubble parameters ratio $R = (0.65, 0.69, 0.73)$, boundary redshift $z_1 = (0.21, 0.23, 0.25)$ and inner matter density profile = (A, B, C, D) (See Table 1 for detail). The variation in confidence contours are examined and explained, and generally, our conclusions are similar to Tomita's.

In Figure 3.5, we plot the 68.3% and 95.4% confidence contours for $R = 0.65$, 0.69 and 0.73, assuming $z_1 = 0.23$, $\alpha = 1$ and matter density profile A. As seen from the figure, when R increases the confidence contours move in the direction of decreasing Ω_{out} and increasing Ω_λ. We perceive this variation because as the Hubble contrast R approaches 1, the level of inhomogeneity of the model falls off, and the confidence contours approach that of the homogeneous Concordance model (Figure 11 in Ref. [8]).

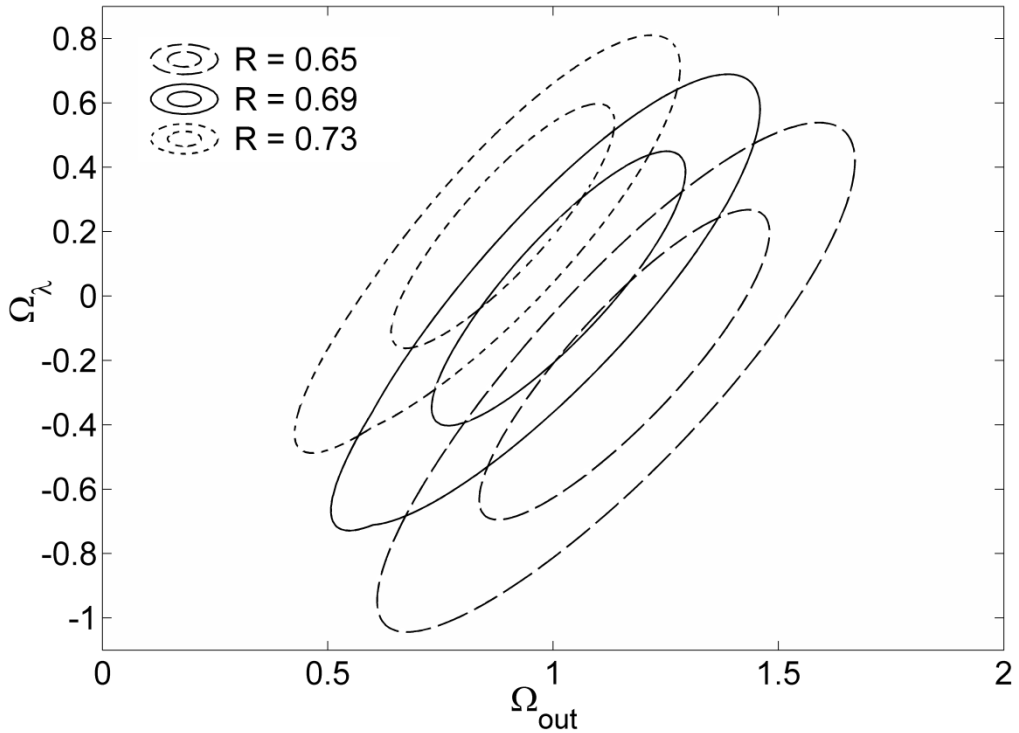

Figure 3.5 68.3% and 95.4% CL contours in $\Omega_{\text{out}} - \Omega_\lambda$ plane, for $R = (0.65, 0.69, 0.73)$, $z_1 = 0.23$, matter density profile A and $\alpha = 1$

Next, we vary z_1 about the standard value $z_1 = 0.23$ and explore the variation of the confidence contours with z_1. We obtain Figure 3.6 below (refer to the Appendix for the Matlab programming codes). We find that the confidence contours have a tendency to move toward larger best-fit Ω_{out} and Ω_λ as z_1

increases. Increasing z_1 in effect increases the size of the local void, and consequently the local void is less dense than the outer region. Apparently, when the size of the low-density local region increases, the total density of the outer region has to increase accordingly for the Hubble diagram to maintain a good fit to the Sne Ia data.

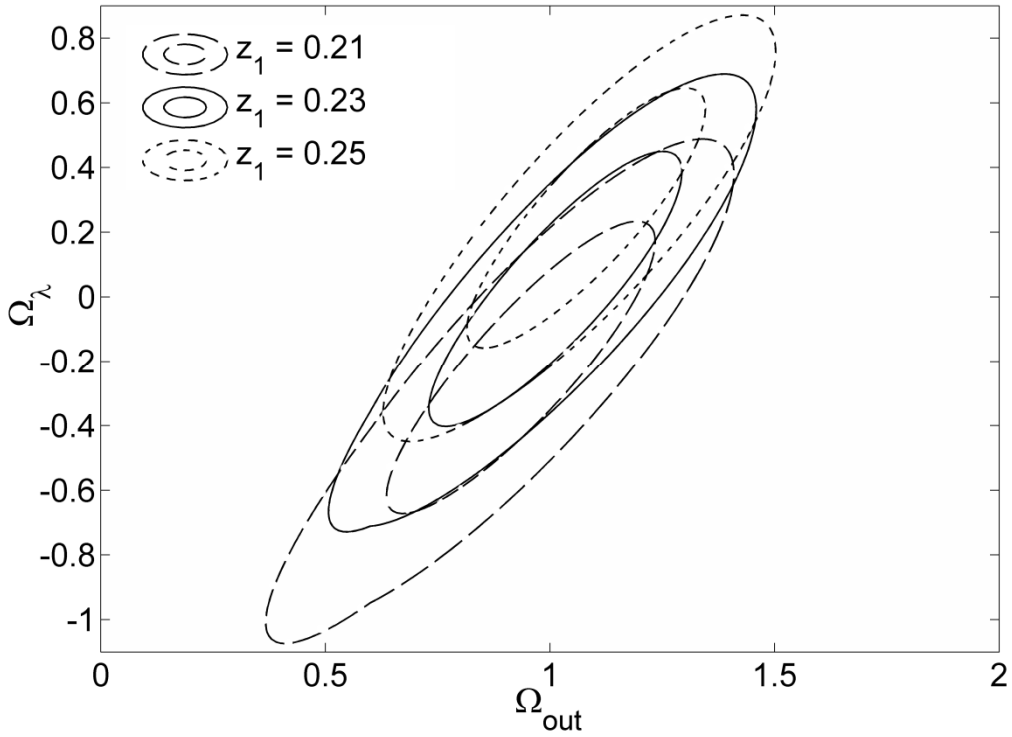

Figure 3.6 Confidence contours at 68.3% and 95.4% CL in $\Omega_{\text{out}} - \Omega_\lambda$ plane for $R = 0.69$, $z_1 = (0.21, 0.23, 0.25)$, matter density profile A and $\alpha = 1$

To understand the variation of the contours in Figure 3.6, we plot the residual Hubble diagrams for various combinations of z_1, Ω_{out} and Ω_λ and show them in Figure 3.7. Note that most of the Sne Ia (over 95%) of the Union compilation lie within the redshift range (0, 1.3), therefore we shall concentrate on the changes in this part of the residual Hubble diagram. We assume that all the observational data points are on the curve which corresponds to the standard parameter case. As can be seen from Figure 3.7, when z_1 increases, the residual

Hubble diagram shifts downward; when Ω_{out} and Ω_{λ} increase, the residual Hubble diagram shifts upward, which almost compensates the downward shift due to the increase in z_1. Accordingly, in Figure 3.6, when z_1 increases, the confidence contours have to move toward higher values of Ω_{out} and Ω_{λ} to get a good fit. Matlab program for generating Figure 3.7 is shown in the Appendix IV.

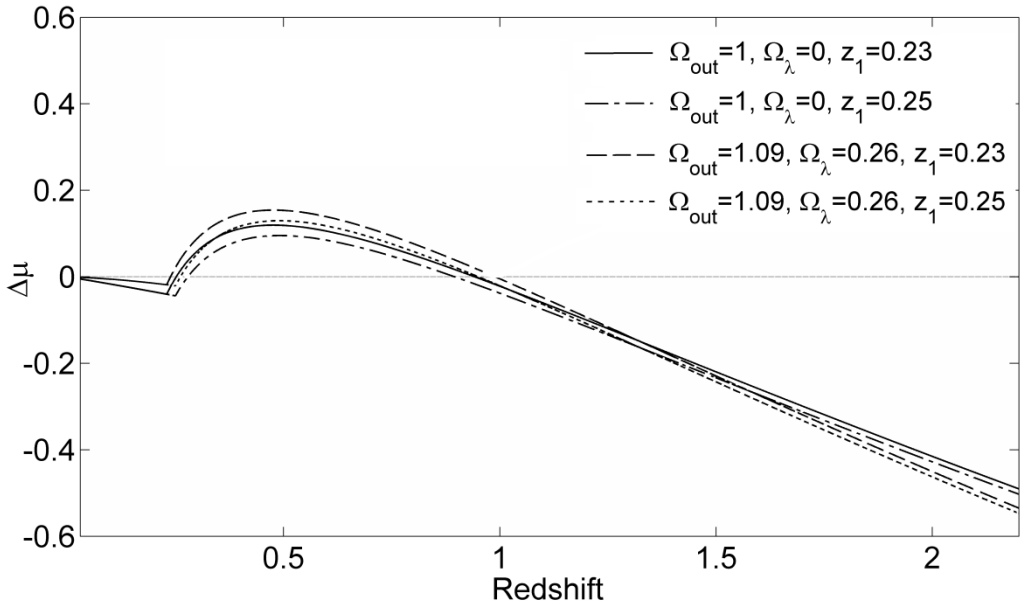

Figure 3.7 The $\Delta\mu - z$ diagram of Tomita's model with four different sets of parameters. The horizontal line corresponds to the empty Milne Universe.

R	z_1	Ω_{out}	Ω_{λ}	χ^2_{min}
0.65	0.23	$1.17^{+0.21}_{-0.22}$	$-0.19^{+0.31}_{-0.33}$	317.51
0.69	0.21	$0.95^{+0.19}_{-0.21}$	$-0.19^{+0.28}_{-0.31}$	316.54
0.69	0.23	$1.02^{+0.18}_{-0.19}$	$0.04^{+0.28}_{-0.29}$	316.04
0.69	0.25	$1.09^{+0.17}_{-0.18}$	$0.26^{+0.26}_{-0.27}$	315.42
0.73	0.23	$0.90^{+0.16}_{-0.17}$	$0.24^{+0.24}_{-0.26}$	314.66

Table 3. Best-fit Ω_{out} and Ω_{λ} with 1σ statistical errors, and χ^2_{min} for different values of R and z_1.

In Table 3, we list the best-fit Ω_{out}, Ω_{λ} and minimum χ^2 for the confidence contours in Figures 3.5 and 3.6. The χ^2 per degree of freedom (dof = 305) only

varies a little from one model to another.

Up to now, we only use profile A for data fitting. This fact could lead us to incorrect conclusions if fitting results are sensitive to this particular choice. Therefore, for completeness, we also examine the best-fit values and confidence contours for various other matter density profiles. Figure 3.8 below shows the contours of four matter density profiles A, B, C, D (see Table 1) and Table 4 summarizes their best-fit values. Interestingly, profile C (with constant $\Omega_{\text{in}} = 0.3$) and A have the same best-fit values and their contours almost overlap. Profile B (with different inner and outer Hubble constant but homogeneous matter density) and profile D (with constant $\Omega_{\text{in}} = 0.2$) give best-fit values and confidence contours only slightly different from that of profile A. Apparently, the confidence contours only vary little and therefore, our results are not sensitive to a specific choice of the matter density profile.

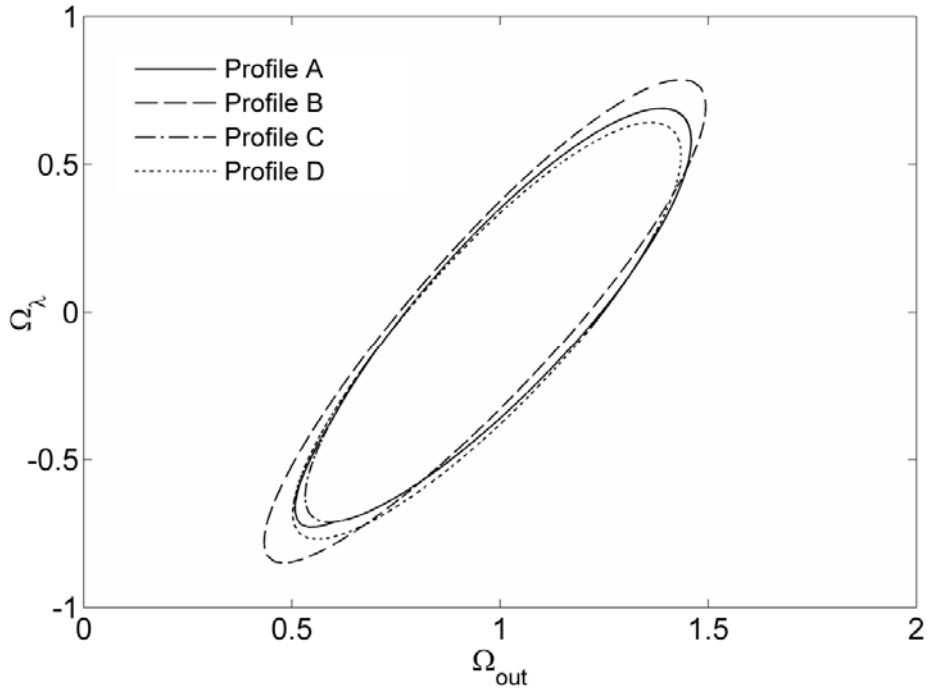

Figure 3.8 Confidence contours at 95.4% CL in $\Omega_{\text{out}} - \Omega_\lambda$ plane for 4 matter density profiles (A, B, C, D) assuming $R = 0.69$, $z_1 = 0.23$, and $\alpha = 1$

Profile	Ω_{out}	Ω_{λ}	χ^2_{min}
A	$1.02^{+0.18}_{-0.19}$	$0.04^{+0.28}_{-0.29}$	316.04
B	$1.01^{+0.20}_{-0.22}$	$0.06^{+0.31}_{-0.35}$	317.28
C	$1.02^{+0.18}_{-0.19}$	$0.04^{+0.28}_{-0.29}$	316.04
D	$1.00^{+0.18}_{-0.20}$	$0.00^{+0.27}_{-0.30}$	315.49

Table 4. Best-fit Ω_{out} and Ω_{λ} with 1σ statistical errors, and χ^2_{min} for different matter density profiles

3.3 The ΛCDM model with clumpiness effect

In previous chapter, we argued that our Universe is in fact clumpy and the light travelling to us mostly propagates through intergalactic medium of a mean matter density smaller than mean value of the whole Universe. The ratio between these two mean matter densities is called clumpiness parameter and denoted by Greek character α. This quantity varies between two extremes: $\alpha = 0$ corresponds to the totally empty intergalactic medium and $\alpha = 1$ corresponds to a smooth Universe. Apart from that, we know the ΛCDM model can not give a good fitting without a non-zero cosmological constant density. So a question is put forward: whether a ΛCDM model taking clumpiness effect into account could explain Sne Ia data without a troublesome cosmological constant or not? In this section, we will find the answer to this issue by performing an examination on the variation of confidence contours of the clumpy ΛCDM model with four values of clumpiness parameter $\alpha = (0.25, 0.50, 0.75, 1.00)$.

Equation (2.29) for calculating angular diameter distance is generally established for both clumpy and smooth Universe with FLRW metric, thus it is correct not only for Tomita's model but also even for ΛCDM model. Therefore, distance modulus – redshift relation in ΛCDM model with clumpiness could be

derived from Eq. (2.29) in which the index j indicating different regions is removed and the initial conditions become $d_a\big|_{z=0} = 0$ and $\left.\frac{dd_a}{dz}\right|_{z=0} = \frac{c}{H_0}$. We use the fitting method in section 2.3 to plot the confidence contours and show the results in Figure 3.9 (Matlab program is provided in the Appendix).

As seen from Figure 3.9, when clumpiness parameter α decreases, the constraining value of the cosmological constant density (Ω_λ) does not fall off, but instead, rises up. Hence, with above tendency of cosmological constant density, we readily realize that adding clumpiness effect to the ΛCDM model is unable to mimic cosmological constant in interpreting Sne Ia data and accelerating expansion. This conclusion, which is drawn from observational evidence, coincides with Teppo Mattsson's theoretical work given in [59].

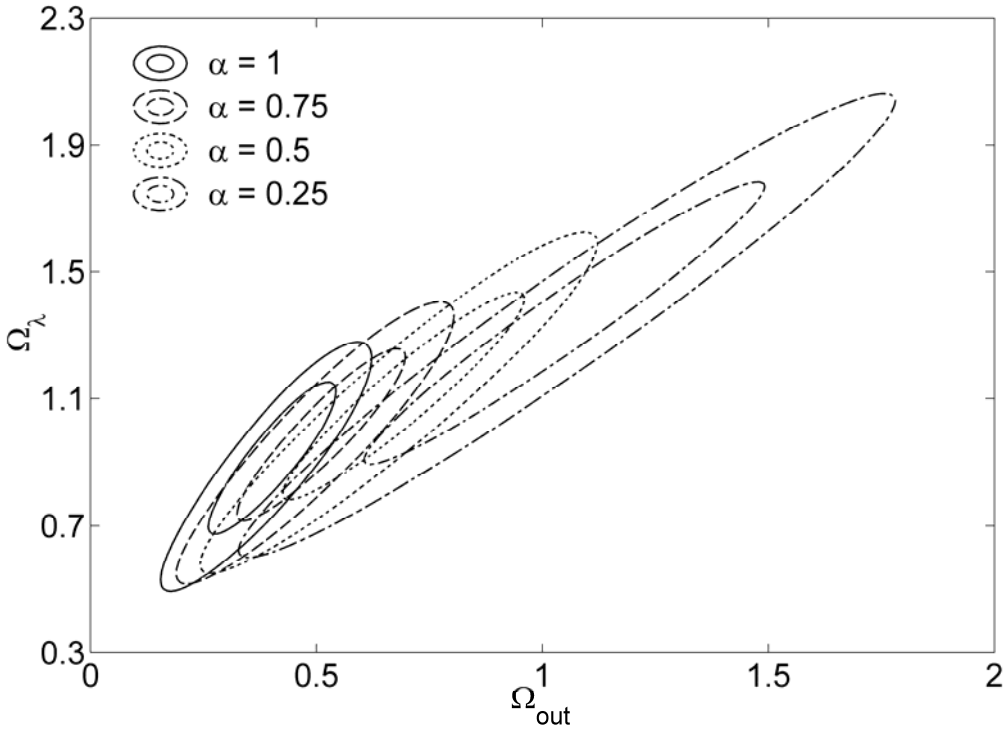

Figure 3.9 68.3% and 95.4% CL contours of α-included ΛCDM model in $\Omega_{\text{out}} - \Omega_\lambda$ plane for four values of clumpiness parameter $\alpha = (0.25, 0.50, 0.75, 1.00)$

3.4 Clumpy Universe and local void's size

In previous parts, we have reasoned that our Universe is not smooth and possibility of $\alpha < 1$ is likely. For Tomita's model with a local void, earlier analyses [35] with the old Sne Ia data only considered the distance modulus – redshift relation in smooth Universe $(\alpha = 1)$ so we do not know what happening to fitting results in clumpy Universe. Therefore, the case of $\alpha < 1$ should be taken into consideration. In this section, we will investigate this general case using the latest released Sne Ia data, SCP Union compilation.

First, we examine the model with identical clumpiness parameters for both the inner and outer region $\alpha_{\text{in}} = \alpha_{\text{out}} \equiv \alpha$ and $\alpha < 1$. We vary parameter α = (0.25, 0.50, 0.75, 1.00) while keeping the other parameters unchanged. In Figure 3.10, we plot the 68.3% CL contours corresponding to the four different values of α listed above.

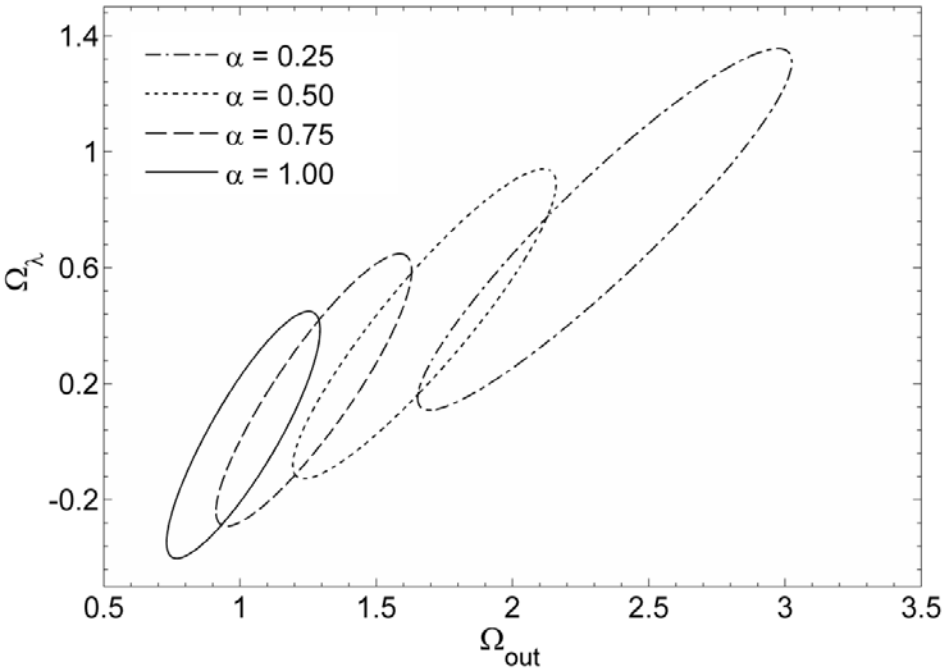

Figure 3.10 68.3% CL contours in $\Omega_{\text{out}} - \Omega_\lambda$ plane for 4 values of clumpiness parameter $\alpha = (0.25, 0.50, 0.75, 1.00)$, with $R = 0.69$ and $z_1 = 0.23$.

In general, as α decreases, the confidence contour widens or in the other words, the constraint on Ω_{out} and Ω_{λ} loosens; the contour also shifts towards larger best-fit Ω_{out} and Ω_{λ} (refer to Table 5). Apparently, when we reduce α, the light will travel through a more dilute medium, increasing densities to keep the product $\alpha\rho$ constant is thus a plausible way to achieve a good fitting as before. This helps to explain the shift of the confidence contours and best-fit values. Interestingly, the contour also shifts in the same direction when we increase the local void size z_1 in the previous case. Hence, by considering $\alpha < 1$, we can reduce the constrained value of local void size z_1. For example, for $\alpha = 0.5$, a smaller local void size $z_1 = 0.16$ is able to provide a reasonably good fit to the SCP Union compilation for $(\Omega_{\text{out}}, \Omega_{\lambda}) \approx (1, 0)$ (see Figure 3.11 and Table 5).

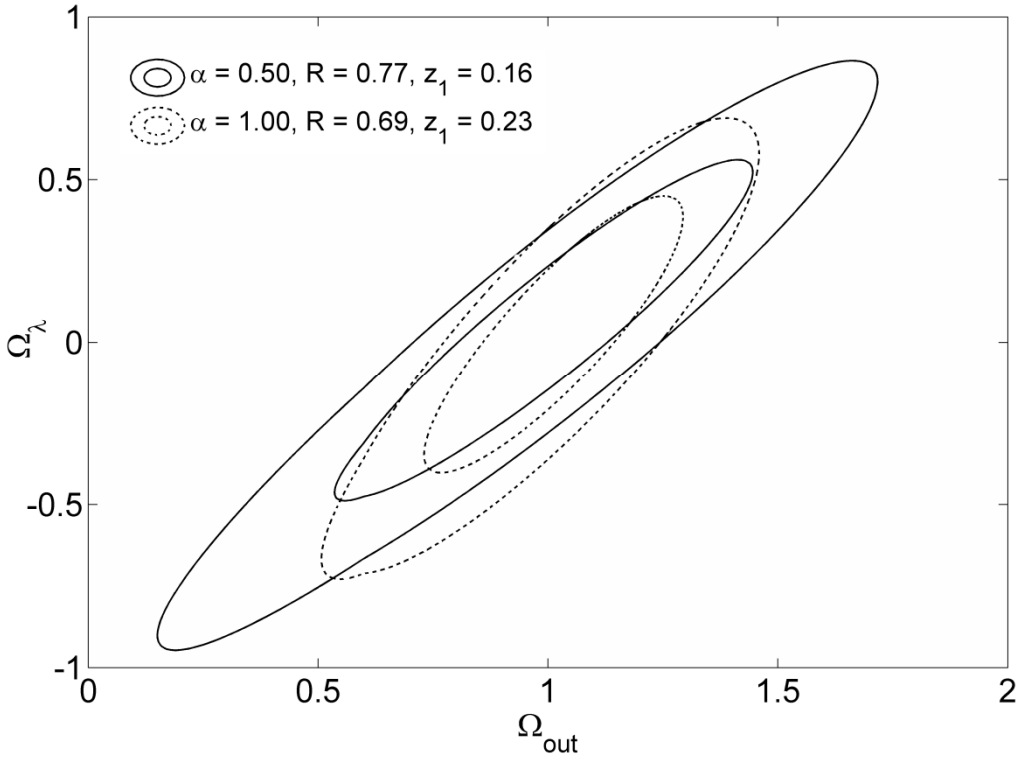

Figure 3.11 68.3% and 95.4% CL contours in $\Omega_{\text{out}} - \Omega_{\lambda}$ plane for the model with standard parameters (dotted line) and with $\alpha = 0.5$, $R = 0.77$ and $z_1 = 0.16$ (solid line).

α	Ω_{out}	Ω_{λ}	χ^2_{min}
0.25	$2.34^{+0.45}_{-0.45}$	$0.75^{+0.40}_{-0.42}$	313.36
0.50	$1.68^{+0.32}_{-0.32}$	$0.42^{+0.35}_{-0.35}$	314.25
0.75	$1.28^{+0.23}_{-0.24}$	$0.20^{+0.30}_{-0.32}$	315.25
1.00	$1.02^{+0.18}_{-0.19}$	$0.04^{+0.28}_{-0.29}$	316.04
0.50	$1.01^{+0.29}_{-0.30}$	$0.06^{+0.33}_{-0.35}$	314.66

Table 5. Best-fit Ω_{out} and Ω_{λ} with 1σ statistical errors, and χ^2_{min}. For the first four rows, $R = 0.69$ and $z_1 = 0.23$; for the last row, $R = 0.77$ and $z_1 = 0.16$.

Altogether, there is a correlation between the clumpiness parameter α and the size of the local void z_1, and an independent measurement of any of the two parameters is required to break this degeneracy.

As defined, clumpiness parameter is the ratio of mean matter density of intergalactic medium to the whole Universe's at a specific time. In the late time, due to gravitational instability, the number of cosmic structures is getting more and more. Accordingly the intergalactic space is getting emptier. Consequently, the level of clumpiness increases according to time and thus clumpiness parameter must be a function of redshift z. The larger the redshift z, the greater the value of clumpiness parameter α. Since objects in the local void are at smaller redshifts than those of outer region and the mean matter density of the local void Ω_{in} is less than outer region's Ω_{out}, in the following part we assume that the clumpiness parameters in each region are constant for simplicity and the one of the local void is always less than or equal to that outside the local void. In the next, to investigate the variation of confidence contours as well as best-fit values in this general case with Sne Ia data, we alter the clumpiness parameters as follows: α_{in} = (0.25, 0.50, 0.75, 1.00) for $\alpha_{\text{out}} = 1.00$ and α_{in} = (0.25, 0.50) for $\alpha_{\text{out}} = 0.50$. The results are shown in Figure

3.12 and 3.13, and Table 6 lists the corresponding best-fit values.

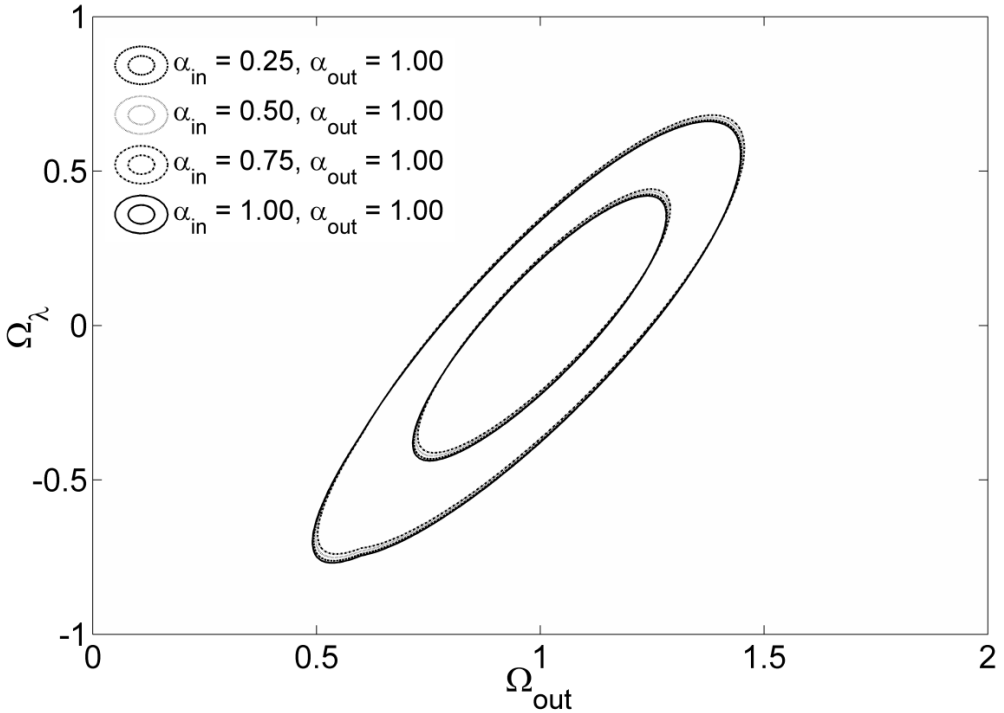

Figure 3.12 68.3% and 95.4% CL contours in $\Omega_{\text{out}} - \Omega_\lambda$ plane for $\{\alpha_{\text{in}}, \alpha_{\text{out}}\} = \{(0.25, 0.50, 0.75, 1.00), 1.00\}$, assuming $R = 0.69$, $z_1 = 0.23$.

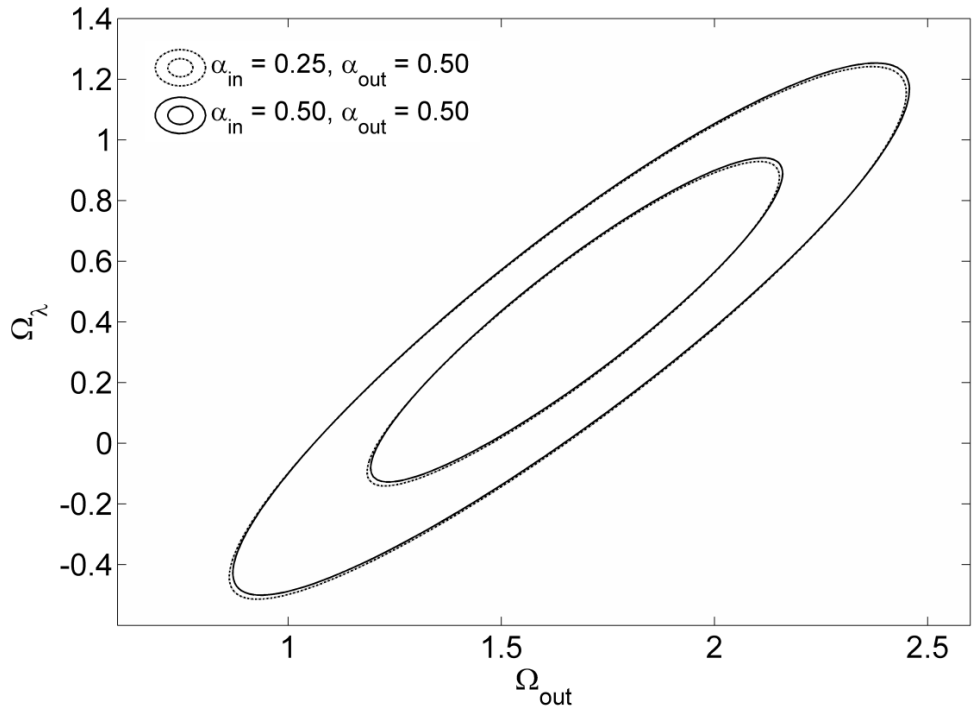

Figure 3.13 68.3% and 95.4% CL contours in $\Omega_{\text{out}} - \Omega_\lambda$ plane for $\{\alpha_{\text{in}}, \alpha_{\text{out}}\} = \{(0.25, 0.50), 0.50\}$, assuming $R = 0.69$, $z_1 = 0.23$.

α_{in}	α_{out}	Ω_{out}	Ω_{λ}	χ^2_{min}
0.25	0.50	$1.68^{+0.31}_{-0.33}$	$0.42^{+0.34}_{-0.37}$	314.28
0.50	0.50	$1.68^{+0.32}_{-0.32}$	$0.42^{+0.35}_{-0.35}$	314.25
0.25	1.00	$1.01^{+0.18}_{-0.19}$	$0.02^{+0.27}_{-0.29}$	315.88
0.5	1.00	$1.01^{+0.19}_{-0.19}$	$0.02^{+0.28}_{-0.28}$	315.93
0.75	1.00	$1.01^{+0.19}_{-0.18}$	$0.04^{+0.27}_{-0.29}$	315.99
1.00	1.00	$1.02^{+0.18}_{-0.19}$	$0.04^{+0.28}_{-0.29}$	316.04

Table 6. Best-fit Ω_{out} and Ω_{λ} with 1σ statistical errors, and χ^2_{min} for $\{\alpha_{\text{in}}, \alpha_{\text{out}}\} = \{(0.25, 0.50, 0.75, 1.00), 1.00\}$ and $\{\alpha_{\text{in}}, \alpha_{\text{out}}\} = \{(0.25, 0.50), 0.50\}$, assuming $R = 0.69$, $z_1 = 0.23$

It is found that in both cases of $\alpha_{\text{out}} = 0.5$ and 1, the confidence contours and best-fit values are almost unchanged as varying the value of clumpiness parameter of the local void. This is apparently true for other values of α_{in} as well as α_{out}. Therefore, we conclude the clumpiness of the local void has little effect on the Sne Ia data fitting. Moreover, in combination with Figure 3.10, we deduce that the variation of α_{out} has a much stronger impact than α_{in} on the constraint of the model parameters.

To summarize, in this section we have investigated the Tomita's model in clumpy Universe in both cases: $\alpha_{\text{in}} = \alpha_{\text{out}} \equiv \alpha$ and $\alpha_{\text{in}} \leq \alpha_{\text{out}} \leq 1$. In the first case, we find that the fitting results are very sensitive to the value of α and there exists a degeneracy between α and z_1. Particularly, the constrained local void size z_1 could be smaller if the value of the clumpiness parameter is indeed less than 1. For example, with $\alpha = 0.5$, the local void boundary's redshift is $z_1 = 0.16$. In the second case, $\alpha_{\text{in}} \leq \alpha_{\text{out}} \leq 1$, the clumpiness of the local void is proven to affect little on the data fitting whereas the value of α_{out} has a strong impact on the constraint of the model parameters.

CHAPTER 4
DISCUSSION

In this work, we study an inhomogeneous model proposed by Tomita. It is an easily visualized, simple inhomogeneous model, based on the likely fact that we are living in a local void surrounded by a wall of galaxies. The simplified assumption that the inner and outer region are homogeneous makes the model easily examined and analyzed.

In our Sne Ia constraints on the Tomita's model, we assume an Einstein-de Sitter (E-dS) cosmology outside the local void and found a low best-fit Hubble constant $h \sim 0.5$. In a recent study, H. Alnes, M. Amarzguioui and Ø. Grøn [37] showed that an Einstein-de Sitter (E-dS) cosmology with a low value of $h \sim 0.5$ could fit the location of first peak in the CMB power spectrum. In another study, P. Hunt and S. Sarkar [60] demonstrated that if the primordial power spectrum is enhanced in the region of second and third acoustic peak, then an E-dS universe with $h \sim 0.44$ will match the Wilkinson Microwave Anisotropy Probe (WMAP) [9, 10] data. The E-dS models with other different additional assumptions [38, 61] have been showed to fit the WMAP data. Therefore, our Sne Ia constraint on Tomita's model is likely to conform with observations from cosmic microwave background radiation, and further studies need to be done to verify this speculation.

In this work, we also found that current observations are still insufficient to distinguish the ΛCDM model and Tomita's model. To discriminate Tomita's model

over ΛCDM model, more detailed observations and investigations are needed to find solid evidences that we live in a local void. A local void, with smaller matter density in comparison to the outside, could be detected by counting galaxies up to very large distances and over a wide area in the sky. With this observation, we can also estimate the scale of the local void size and put a more stringent constraint on the matter density difference between the two regions.

In addition, more precise Sne Ia observations can be conducted to distinguish the residual Hubble diagram of Tomita's model and ΛCDM model. In particular, due to the existence of the shell, the residual Hubble diagram of Tomita's model (Figure 3.2 and 3.7) contains a "sharp" transition between the inner and outer region in the redshift range of 0.1 to 0.4 approximately, therefore more precise Sne Ia observations in this redshift range will support or reject the local void in Tomita's model. Moreover, the disparity between the Hubble diagrams is large at high redshifs, therefore more precise Sne Ia observations at high redshifts are necessary, although high-redshift Sne Ia are usually very faint and hard to observe precisely.

Lastly, we need to emphasize that the Tomita's model that we consider in this work is not truly a realistic model. It is simply a toy model, used to prove the idea that non-linear structures play a role in the interpretation of cosmological data. Future work can carry out a more realistic and careful investigation on the inhomogeneous model. For example, future fitting can consider a non-spherical local void and an off-center observer. In addition, one can consider the shell's thickness and, accordingly, the effect of shell's mass on surrounding spacetime and the shell's impact on light propagation through the transitional region. An even more practical model may have a smooth transitional region. Furthermore, the clumpiness

parameter α, where $\rho = \alpha \rho_{mean\_Universe}$, should be a function of redshift z. For example, recently in T. Mattsson's model [59] the author assumed $H(z) = \beta(z) H_{FLRW}(z) \left(\beta(z) \geq 1\right)$, where $H_{FLRW}(z)$ represents the usual Hubble rate in Friedmannian Universe and the local expansion rate depends on the local matter density, we can also make similar assumption to the Tomita's model.

CHAPTER 5
CONCLUSIONS

As of today, there have been many attempts to prove that cosmic inhomogeneity is able to mimic dark energy in some cosmological observations. Many have considered the LTB model, and fitted the Sne Ia data without the cosmological constant. Nevertheless, to better demonstrate that the accelerating expansion of the universe is only an apparent phenomenon caused by inhomogeneous distribution of matter in space, some have considered other more realistic cosmological models [60-67].

In this thesis, we consider a simple inhomogenous model with a local void (proposed by Tomita), and our aim is to update the Sne Ia constraint using the latest SCP Union supernovae compilation. For the model to fit the latest Sne Ia data, it has been found by others that the local void has to be large, on scales of Gpc [37, 38, 45]. In our work, we find that the small local void on scale of about 200 Mpc from an early constraint does not fit well to the SCP Union supernovae compilation when $(\Omega_{\text{out}}, \Omega_{\lambda}) = (1, 0)$. When $(\Omega_{\text{out}}, \Omega_{\lambda}) = (1, 0)$ is a pre-requirement, we find the best-fit parameters $R = 0.69$ and $z_1 = 0.23$, correspond to a large local void on scale of about 1 Gpc. Although the existence of the large void in the universe is physically unlikely (according to standard theory of structure formation), there have been a lot of observational evidences [19-22] for the existence of voids, and recently Hunt and

Sarkar [68] have argued the credibility of dismissing local void on the ground of being inconsistent with the standard theory of structure formation.

With the latest Sne Ia dataset, we have also re-investigated the variation of confidence contours and best-fit values on model parameters, and the results of our investigation are in general similar to that of Tomita's previous investigation using an older dataset. We have also proven that the choice of matter density profile does not strongly affect our results.

In this study, we also consider the more general case that $\alpha < 1$. We find that the results of data fitting strongly depend on the value of α, such that the smaller the value of α, the smaller the best-fit size of the local void. Besides, we also investigate different clumpiness parameters for different regions $\left(\alpha_{\text{in}} \neq \alpha_{\text{out}}\right)$ and show that the value of α_{in} does not affect the fitting as much as α_{out} does.

In this work we only use the Sne Ia data to constrain the model parameters. Future studies can confront the model with other independent observations such as CMB, BAO, BBN (Big Bang Nucleosynthesis), etc., to cross-check the model, break the degeneracy and provide a tighter constraint to the parameters.

Bibliography

1. A. G. Riess, A. V. Filippenko, P. Challis *et al.*, *AJ* **116**, 1009 (1998).
2. B. P. Schmidt, N. B. Suntzeff, M. M. Phillips *et al.*, *ApJ* **507**, 46 (1998).
3. S. Perlmutter, G. Aldering, G. Goldhaber *et al.*, *ApJ* **517**, 565 (1999).
4. A. G. Riess, L. G. Strolger, J. Tonry *et al.*, *ApJ* **607**, 665 (2004).
5. P. Astier, J. Guy, N. Regnault *et al.*, *A&A* **447**, 31 (2006).
6. A. G. Riess, L. G. Strolger, S. Casertano *et al.*, *ApJ* **659**, 98 (2007).
7. W. M. Wood-Vasey, G. Miknaitis, C. W. Stubbs *et al.*, *ApJ* **666**, 694 (2007).
8. M. Kowalski, D. Rubin, G. Aldering *et al.*, *ApJ*, 749 (2008).
9. D. N. Spergel, L. Verde, H. V. Peiris *et al.*, *ApJS* **148**, 175 (2003).
10. D. N. Spergel, R. Bean, O. Dore *et al.*, *ApJS* **170**, 377 (2007).
11. J. Dunkley, E. Komatsu, M. R. Nolta *et al.*, *ApJS* **180**, 306 (2009).
12. D. J. Eisenstein, I. Zehavi, D. W. Hogg *et al.*, *ApJ* **633**, 560 (2005).
13. S. Ho, C. Hirata, N. Padmanabhan *et al.*, *arXiv* **0801.0642** (2008).
14. M. Roos, *Introduction to cosmology* (Wiley, 2003).
15. M. Dabrowski and M. Hendry, *ApJ* **498**, 67 (1998).
16. M. N. Celerier, *A&A* **353**, 63 (2000).
17. K. Tomita, *ApJ* **529**, 38 (2000).
18. E. Copeland, M. Sami, and S. Tsujikawa, *IJMPD* **15**, 1753 (2006).
19. W. J. Frith, G. S. Busswell, R. Fong *et al.*, *MNRAS* **345**, 1049 (2003).
20. I. Zehavi, Adam G. Riess, Robert P. Kirshner *et al.*, *ApJ* **503**, 483 (1998).
21. I. J. Richard Gott, J. Mario, S. David *et al.*, 2005), p. 463.

22. B. R. Granett, M. C. Neyrinck, Istv *et al.*, *ApJ*, L99 (2008).

23. P. Vielva, E. Martínez-González, R. Barreiro *et al.*, *ApJ* **609**, 22 (2004).

24. M. Cruz, M. Tucci, E. Martinez-Gonzalez *et al.*, *MNRAS* **369**, 57 (2006).

25. M. Cruz, L. Cayon, E. Martinez-Gonzalez *et al.*, *ApJ* **655**, 11 (2007).

26. L. Rudnick, S. Brown, and L. R. Williams, *ApJ*, 40 (2007).

27. K. T. Inoue and J. Silk, *ApJ*, 23 (2006).

28. M. F. Shirokov and I. Z. Fisher, *AZh* **39**, 899 (1962).

29. G. F. R. Ellis, *Gen. Rel. Grav. (A86-12326 02-90). Dordrecht, D. Reidel Publishing Co.*, 73 (1984).

30. T. Buchert, *Gen. Rel. Grav.* **32**, 105 (2000).

31. S. Räsänen, *JCAP* **11**, 003 (2006).

32. T. Buchert, *Gen. Rel. Grav* **40**, 467.

33. T. Biswas, R. Mansouri, and A. Notari, *JCAP* **12**, 017 (2007).

34. S. Alexander, T. Biswas, A. Notari *et al.*, *arXiv* **0712.0370** (2007).

35. K. Tomita, *PThPh* **106**, 929 (2001).

36. K. Tomita, *MNRAS* **326**, 287 (2001).

37. H. Alnes, M. Amarzguioui, and O. Gron, *Phys. Rev. D* **73** (2006).

38. J. Garcia-Bellido and T. Haugbolle, *JCAP*, 003 (2008).

39. J. P. Zibin, A. Moss, and D. Scott, *Phys. Rev. Lett.* **101**, 251303 (2008).

40. K. Enqvist, *Gen. Rel. Grav.* **40**, 451 (2008).

41. M. N. Celerier, *arXiv* **astro-ph/0702416** (2007).

42. G. Lemaitre, *Ann. Soc. Sci. Brux. Ser. Sci. Math. Astron. Phys. A* **53**, 51 (1933).

43. R. C. Tolman, *Proc. Nat. Acad. Sci.* **20**, 169 (1934).

44. H. Bondi, *Gen. Rel. Grav.* **31**, 1783 (1999).

45. T. Clifton, P. Ferreira, and K. Land, *Phys. Rev. Lett.* **101**, 131302 (2007).

46. K. Tomita, *ApJ* **529**, 26 (2000).

47. C. C. Dyer and R. C. Roeder, *ApJ* **174** (1972).

48. C. C. Dyer and R. C. Roeder, *ApJ* **180** (1973).

49. M. McClure and C. Dyer, *New Astronomy* **12**, 533 (2007).

50. S. Sakai, J. Mould, S. Hughes *et al.*, *ApJ* **529**, 698 (2000).

51. W. Freedman, B. Madore, B. Gibson *et al.*, *ApJ* **553**, 47 (2001).

52. C. Kochanek, *Arxiv* **astro-ph/0204043** (2002).

53. C. Kochanek, *ApJ* **578**, 25 (2002).

54. E. Reese, J. Mohr, J. Carlstrom *et al.*, *ApJ* **533**, 38 (2000).

55. M. Tada and T. Futamase, *PThPh* **104**, 971 (2000).

56. R. Sachs, *Proc. R. Soc. Lond. A* **264**, 309 (1961).

57. E. Poisson, *A relativist's toolkit: the mathematics of black-hole mechanics* (Cambridge University Press, 2004).

58. P. Peebles, *Principles of physical cosmology* (Princeton University Press, 1993).

59. T. Mattsson, *arXiv* **astro-ph/0711.4264** (2007).

60. P. Hunt and S. Sarkar, *Phys. Rev. D* **76**, 123504 (2007).

61. A. Blanchard, M. Douspis, M. Rowan-Robinson *et al.*, *A&A* **412**, 35 (2003).

62. D. L. Wiltshire, *Phys. Rev. Lett.* **99**, 251101 (2007).

63. D. L. Wiltshire, *New Journal of Physics* **9**, 377 (2007).

64. D. L. Wiltshire, *IJMPD* **17**, 641 (2008).

65. B. M. Leith, S. C. C. Ng, and D. L. Wiltshire, *ApJ*, L91 (2008).

66. A. Blanchard, M. Douspis, M. Rowan-Robinson *et al.*, *A&A* **449**, 925 (2006).

67. P. Hunt and S. Sarkar, *Phys. Rev. D* **70**, 103518 (2004).

68. P. Hunt and S. Sarkar, *Arxiv* **astro-ph/0807.4508** (2008).

Appendix: Matlab programs

I. Matlab programming codes for finding best-fit Ω_{out}, Ω_{λ}, minimum χ^2 and plotting corresponding confidence contours of Tomita's model with a set of specific values of $R \equiv H_{\text{out}}/H_{\text{in}}$, z_1, Ω_{in}, and α.[1]

1. Main program

```
clear all;close all;clc;
% load data file
data=load('SCPUnion.txt');
z=data(:,1);
muy=data(:,2);
sigma_muy=data(:,3);
% ---------
% set parameters
c=3e5;
z1=0.23;                          % redshift of boundary;
z_max=max(z);
alpha=1;                          % clumpiness parameter;
% in case of alpha_in ≠ alpha_out, replace above statement with values of alpha_in and
% alpha_out
R=0.69;                           % Hubble rates' ratio
omega_min=0; omega_max=2;         % omega_out's value range
delta_omega=0.01;                 % omega_out's jump step
lambda_min=-1;lambda_max=1;       % omega_lambda's value range
```

[1] Thereafter, we use the standard values of parameters R, α, z_1 and matter density profile. For other cases, we simply change the old values by the new ones.

```
delta_lambda=0.01;                  % omega_lambda's jump step
H_min=60;H_max=80;                  % Hubble rate's value range
delta_H=0.1;                        % Hubble rate's jump step
% ---------
i=0;
for omega_out=omega_min:delta_omega:omega_max
   % set matter density profile A
   if omega_out>0.6
      omega_in=0.30;
   else
      omega_in=omega_out/2;
   end
   %---------
   i=i+1;
   j=0;
   for lambda_out=lambda_min:delta_lambda:lambda_max
      j=j+1;
      lambda_in=lambda_out*R^2;
      poly1=[omega_in,1+2*omega_in-lambda_in,2+omega_in-2*lambda_in,1];
      poly2=[omega_out,1+2*omega_out-lambda_out,2+omega_out-...
                                                    2*lambda_out,1];
      sol_poly1=find_pos_sol(sort(roots(poly1)));
      sol_poly2=find_pos_sol(sort(roots(poly2)));
      counter1=count(sol_poly1,z1);
      counter2=count(sol_poly2,z_max);
      if counter1~=0 || counter2~=0
         chisq(i,j)=9999;
      else
         da_in=da1(omega_in,lambda_in,1,c,alpha,z1); % change "alpha" in this
                                % statement into "alpha_in" in case of α_in ≠ α_out
         ini_condition=inicond(da_in,omega_out,lambda_out,R,c,alpha,z1);
```

```
% change “alpha” in above statement into “alpha_out” in case of α_in ≠ α_out
da_out=da2(omega_out,lambda_out,ini_condition,alpha,z1,z_max);
sign=0;
for k=1:length(z)
   if z(k)<=z1
      DL(k)=distance(da_in,z(k));
   else
      DL(k)=distance(da_out,z(k));
   end
   if DL(k)<0
      sign=1;
      break;
   end
end
if sign==1
   chisq(i,j)=9999;
else
   l=0;
   for H_in=H_min:delta_H:H_max
      H_out=H_in*R;
      l=l+1;
      chisqH(l)=0;
      for m=1:length(z)
         if z(m)<=z1
           muy_prd=5*log10(DL(m)/H_in)+25;
         else
          muy_prd=5*log10(DL(m)/H_out)+25;
         end
         chisqH(l)=chisqH(l)+(muy_prd-muy(m))^2/sigma_muy(m)^2;
      end
   end
   A=exp(-chisqH/2);
```

```
            chisq(i,j)=-2*log(trapz(A)*delta_H);
        end
    end
  end
end
%---------
% confidence contours plot
x=omega_min:delta_omega:omega_max;
y=lambda_min:delta_lambda:lambda_max;
[xx,yy]=meshgrid(x,y);
minchisq=min(min(chisq));
[i,j]=find(chisq==minchisq);
zz=transpose(chisq-minchisq);
[cc1,hh1]=contour(xx,yy,zz,[1,2.30,6.18]); % the contour corresponding to Δχ^2 = 1
                                           % is used for determining the statistical
                                           % errors of Ω_out and Ω_λ .
sprintf('%s:%f\n%s:%f\n%s:%f','best-fit omega_out',x(i),'best-fit...
                              omega_lambda',y(j),'minimum chisquare',minchisq)
```

2. Sub-functions of the main program

a. function *find_pos_sol*

```
% find real, positive and different elements in the matrix sol_poly
function result=find_pos_sol(sol_poly) % sol_poly is the solutions of a polynomial
switch length(sol_poly)
  case 0
    result=[];
  case 1
    if abs(imag(sol_poly))<1e-6 && sol_poly>0
      result=sol_poly;
    else
      result=[];
```

```
    end
case 2
    if abs(imag(sol_poly(1)))>1e-6 || sol_poly(1)<0
        result=sol_poly(2);
        if abs(imag(sol_poly(2)))>1e-6 || sol_poly(2)<0
            result=[];
        end
    else
        result=sol_poly(1);
        if abs(imag(sol_poly(2)))<1e-6 && sol_poly(2)>0
            result=sol_poly;
        end
    end
case 3
    if abs(imag(sol_poly(1)))>1e-6 || sol_poly(1)<0
        result=[sol_poly(2) sol_poly(3)];
        if abs(imag(sol_poly(2)))>1e-6 || sol_poly(2)<0
            result=sol_poly(3);
            if abs(imag(sol_poly(3)))>1e-6 || sol_poly(3)<0
                result=[];
            end
        elseif abs(imag(sol_poly(3)))>1e-6 || sol_poly(3)<0
                result=sol_poly(2);
        end
    else
        result=sol_poly;
        if abs(imag(sol_poly(2)))>1e-6 || sol_poly(2)<0
            result=[sol_poly(1) sol_poly(3)];
            if abs(imag(sol_poly(3)))>1e-6 || sol_poly(3)<0
                result=sol_poly(1);
            end
        elseif abs(imag(sol_poly(3)))>1e-6 || sol_poly(3)<0
```

```
            result=[sol_poly(1) sol_poly(2)];
        end
    end
end
result=real(result);
switch length(result)
  case 2
    if result(1)==result(2)
        result=result(1);
    end
  case 3
    if result(1)==result(2)
        if result(2)==result(3)
            result=result(1);
        else
            result=[result(1),result(3)];
        end
    else
        if result(2)==result(3)
            result=[result(1) result(3)];
        else
            if result(1)==result(3)
                result=[result(1) result(2)];
            end
        end
    end
end
```

b. Function *count*

```
%count the number of elements of sol_poly satisfied sol_poly<z
function counter=count(sol_poly,z)
counter=0;
```

```
for k=1:length(sol_poly)
   if sol_poly(k)<=z
      counter=counter+1;
   end
end
```

c. Function *da1*

```
% solving diffential equation of angular diameter distance in region I from z_min=0
% to z_max=z1
function sol1=da1(omega_in,lambda_in,H01,c,alpha,z1)
f1=@(z)(1+omega_in*z)*(1+z)^2-lambda_in*z*(2+z);
dy=@(z,y)[y(2);-(2/(1+z)+1/2*(1+z)*(omega_in*(1+3*z)+2-2*lambda_in)/f1(z))*...
                                        y(2)-3/2*omega_in*alpha*(1+z)/f1(z)*y(1)];
options=odeset('RelTol',1e-4,'AbsTol',1e-7);
sol1=ode45(dy,[0 z1],[0;c/H01],options);
```

d. Function *inicond*

```
% finding initial conditions of the angular diameter distance in region II
function result=inicond(sol1,omega_out,lambda_out,ratio,c,alpha,z1)
bcda21=ratio*deval(sol1,z1,1);
bcda22=c;
f2=@(z)(1+omega_out*z)*(1+z)^2-lambda_out*z*(2+z);
daode=@(z,y)[y(2);-(2/(1+z)+1/2*(1+z)*(omega_out*(1+3*z)+...
        2-2*lambda_out)/f2(z))*y(2)-3/2*omega_out*alpha*(1+z)/f2(z)*y(1)];
dabc=@(ya,yb)[ya(2)-bcda22;yb(1)-bcda21];
dajac=@(z,y)[0,1;-3/2*omega_out*alpha*(1+z)/f2(z),-(2/(1+z)+1/2*...
                        (1+z)*(omega_out*(1+3*z)+2-2*lambda_out)/f2(z))];
solinit=bvpinit(linspace(0,z1,11),[bcda21;bcda22]);
options=bvpset('RelTol',1e-4,'AbsTol',1e-7,...
                                        'Fjacobian',dajac,'BCJacobian',@dabcjac);
sol=bvp4c(daode,dabc,solinit,options);
dda2dz=deval(sol,z1,2);
result=[bcda21;dda2dz];
```

```
%---------
        % jacobian dabcjac for solving differential equation
        function [dbcdya,dbcdyb]=dabcjac(ya,yb)
        dbcdya=[0,1;0,0];
        dbcdyb=[0,0;1,0];
        %---------
```

e. Function *da2*

```
% solving the diffential equation of angular diameter distance  in region II from
% z_min=z1 to z_max=z_max
function sol2=da2(omega_out,lambda_out,inicond,alpha,z1,z_max)
f2=@(z)(1+omega_out*z)*(1+z)^2-lambda_out*z*(2+z);
dy=@(z,y)[y(2);-(2/(1+z)+1/2*(1+z)*(omega_out*(1+3*z)+2-...
                2*lambda_out)/f2(z))*y(2)-3/2*omega_out*alpha*(1+z)/f2(z)*y(1)];
options=odeset('RelTol',1e-4,'AbsTol',1e-7);
sol2=ode45(dy,[z1,z_max],inicond,options);
```

f. Function *distance*

```
% calculating the luminosity distance and its derivative at redshift z with angular
% diameter distance in (0,z1) given by da
function [dl ddl_dz]=distance(da,z)
sol=deval(da,z);
dl=(1+z)^2*sol(1);
ddl_dz=2*(1+z)*sol(1)+(1+z)^2*sol(2);
```

II. Matlab codes for binning observational data (SCP Union compilation) and plotting corresponding $\Delta\mu - z$ diagram

```
% finding the boundary points of each bin with n*delta(z)=Const
% calculating the mean of redshift, delta distance modulus and sigma
% plotting the diagram with error bars.
clear all;close all;clc;
data=load('SCPUnion.txt');
```

```
z=data(:,1);
muy=data(:,2);
sigma_muy=data(:,3);
z_max=max(z);
c=3e5;
H0=68.5;
% ---------
% find the boundary points of bins
C=10;
delta_C=0.1;
sign1=1;
count=1;
zr=0;
binpoint(1)=zr; % left boundary of the first bin
delta_z=0.00001;
while (sign1==1)
   z0=zr;
   sign2=1;
   while (sign2==1)
      zr=zr+delta_z;      % running variable
      lgt=length(find((z0<=z)&(z<=zr)));
      if lgt*(zr-z0)>C-delta_C&&lgt*(zr-z0)<C+delta_C
         sign2=0;
      end
      if zr>z_max
         sign1=0;
         sign2=0;
      end
   end
   count=count+1;
   binpoint(count)=zr;
end
```

```
binpoint % boundary points of bins.
% ---------
% calculating average of z, delta_muy and sigma_muy in each bin.
lgt_bp=length(binpoint);
for i=1:lgt_bp-1
   a=find((binpoint(i)<=z)&(z<=binpoint(i+1)));
   sum_z=0;
   sum1=0;
   sum2=0;
   for j=1:length(a)
      sum_z=sum_z+z(a(j));
      N_empty=5*log10(c/H0*z(a(j))*(1+z(a(j))/2))+25;
      sum1=sum1+(muy(a(j))-N_empty)/sigma_muy(a(j))^2;
      sum2=sum2+1/sigma_muy(a(j))^2;
   end
   avg_z(i)=sum_z/length(a);          % average of redshift ⟨z⟩ (in i^th bin)
   avg_delta_muy(i)=sum1/sum2;        % average of delta distance modulus ⟨Δμ⟩
   avg_sigma_muy(i)=sqrt(1/sum2);`% average of distance modulus dispersion ⟨σ⟩
end
avg_z
avg_delta_muy
avg_sigma_muy
errorbar(avg_z,avg_delta_muy,avg_sigma_muy,'*');
```

III. Matlab codes for plotting the residual Hubble diagram of the homogeneous ΛCDM model

```
clear all;close all;clc;
z=0.01:0.01:2.3;
c=3e5;
omega=0.287;          % matter density
lambda=0.713;         % dark energy density in the form of a cosmological constant
```

```
omega_k=1-omega-lambda;
for i=1:length(z)
   N_empty(i)=5*log10(c*(1+z(i))*sinh(log(1+z(i))));
   N_LCDM(i)=5*log10(c*(1+z(i))*quad(@(x)1./sqrt((1+x).^2.*(1+omega.*x)-…
                                                    x.*(2+x).*lambda),0,z(i)));
end
delta_N=N_LCDM-N_empty;
plot(z,delta_N);
```

IV. Matlab codes for plotting the residual Hubble diagrams of Tomita's model

```
clear all;close all;clc;
z=0.01:0.001:2.3;
c=3e5;
zmax=max(z);
omega_in=0.3;
omega_out=1;
ratio=0.69;
lambda_out=0;
lambda_in=lambda_out*ratio^2;
z1=0.23;
alpha=1;
%----------------
poly1=[omega_in,1+2*omega_in-lambda_in,2+omega_in-2*lambda_in,1];
poly2=[omega_out,1+2*omega_out-lambda_out,2+omega_out-2*lambda_out,1];
sol_poly1=find_pos_sol(sort(roots(poly1)));
sol_poly2=find_pos_sol(sort(roots(poly2)));
counter1=count(sol_poly1,z1);
counter2=count(sol_poly2,zmax);
sum=0;
if counter1~=0 || counter2~=0
```

```
    disp('not meaningful value of pair (omega_out;lambda_out). Please change …
                                                                another pair');
else
    da_in=da1(omega_in,lambda_in,1,c,alpha,z1);
    inicondition=inicond(da_in,omega_out,lambda_out,ratio,c,alpha,z1);
    da_out=da2(omega_out,lambda_out,inicondition,alpha,z1,zmax);
    sign=0;
    for i=1:length(z)
        if z(i)<=z1
            DL=distance(da_in,z(i));
        else
            DL=distance(da_out,z(i));
        end
        if DL<0
            sign=1;
            break;
        else
            N_Tomita(i)=5*log10(DL);
        end
    end
    if sign==1
        disp('not meaningful value of pair (omega_out;lambda_out). Please change …
                                                                different pair');
    else
        % Calculating distance modulus of the empty homogeneous Milne Universe
        for i=1:length(z)
            N_empty(i)=5*log10(c*(1+z(i))*sinh(log(1+z(i))));
        end
        for i=1:length(z)
            if z(i)<=z1
                delta_N(i)=N_Tomita(i)-N_empty(i);
            else
```

```
            delta_N(i)=N_Tomita(i)-N_empty(i)-5*log10(ratio);
          end
        end
        plot(z,delta_N);grid on;
    end
end
```

V. Matlab codes for finding best-fit Ω_{out}, Ω_{λ}, minimum χ^2 and plotting corresponding confidence contours of ΛCDM model taking clumpiness effect into account

```
clear all;close all;clc;
% load data file
data=load('SCPUnion.txt');
z=data(:,1);
muy=data(:,2);
sigma_muy=data(:,3);
% ---------
% set parameters
c=3e5;
z_max=max(z);
alpha=0.25;
omega_min=0;omega_max=2;
delta_omega=0.1;
lambda_min=0;lambda_max=3;
delta_lambda=0.1;
H_min=60;H_max=80;
delta_H=0.1;
%---------
i=0;
for omega=omega_min:delta_omega:omega_max
    i=i+1;
```

```
   j=0;
   for lambda=lambda_min:delta_lambda:lambda_max
      j=j+1;
      poly1=[omega,1+2*omega-lambda,2+omega-2*lambda,1];
      sol_poly1=find_pos_sol(sort(roots(poly1)));
      counter=count(sol_poly1,z_max);
      if counter~=0
         chisq(i,j)=9999;
      else
         DA=da1(omega,lambda,1,c,alpha,z_max);
         for k=1:length(z)
            DL(k)=distance(DA,z(k));
         end
         l=0;
         for H0=H_min:delta_H:H_max
            l=l+1;
            chisqH(l)=0;
            for k=1:length(z)
               muy_prd=5*log10(DL(k)/H0)+25;
               chisqH(l)=chisqH(l)+(muy_prd-muy(k))^2/sigma_muy(k)^2;
            end
         end
         A=exp(-chisqH/2);
         chisq(i,j)=-2*log(trapz(A)*delta_H);
      end
   end
end
%---------
% confidence contours plot
x=omega_min:delta_omega:omega_max;
y=lambda_min:delta_lambda:lambda_max;
[xx,yy]=meshgrid(x,y);
```

```
minchisq=min(min(chisq));
[i,j]=find(chisq==minchisq);
zz=transpose(chisq-minchisq);
[cc1,hh1]=contour(xx,yy,zz,[1,2.30,6.18]);
sprintf('%s:%f\n%s:%f\n%s:%f','best-fit omega_out',x(i),...
                              'best-fit omega_lambda',y(j),'minimum chisquare',minchisq)
```